Tectonics

RESEARCH ARTICLE
10.1029/2018TC005158

Key Points:
- Brittle mesostructures analysis contributes to establish the geodynamic evolution of the Fuegian Andes area
- The stress fields establish are congruous with a regional NE-SW compressive stress direction active in the zone since the Late Cretaceous
- Deflection of the regional stress field by large crustal heterogeneities controlled the local structures

Supporting Information:
- Supporting Information S1
- Figure S1
- Table S1
- Table S2
- Table S3

Correspondence to:
A. Maestro,
a.maestro@igme.es

Citation:
Maestro, A., Ruano, P., Torres Carbonell, P., Bohoyo, F., Galindo-Zaldívar, J., Pedrera, A., et al. (2019). Stress field evolution of the southernmost Andean Cordillera from paleostress analysis (Argentine Tierra del Fuego). *Tectonics*, *38*, 7–25. https://doi.org/10.1029/2018TC005158

Received 24 MAY 2018
Accepted 9 NOV 2018
Accepted article online 12 NOV 2018
Published online 1 JAN 2019

Stress Field Evolution of the Southernmost Andean Cordillera From Paleostress Analysis (Argentine Tierra del Fuego)

A. Maestro[1,2], P. Ruano[3,4], P. Torres Carbonell[5], F. Bohoyo[1], J. Galindo-Zaldívar[3,4], A. Pedrera[6], A. Ruiz-Constán[6], L. González-Castillo[3], P. Ibarra[1], and J. López-Martínez[2]

[1]Instituto Geológico y Minero de España, Madrid, Spain, [2]Departamento de Geología y Geoquímica, Facultad de Ciencias, Universidad Autónoma de Madrid, Madrid, Spain, [3]Departamento de Geodinámica, Universidad de Granada, Granada, Spain, [4]Instituto Andaluz de Ciencias de la Tierra, Granada, Spain, [5]Centro Austral de Investigaciones Científicas (CADIC-CONICET), Ushuaia, Argentina, [6]Instituto Geológico y Minero de España, Unibersidad de Granada, Granada, Spain

Abstract The Argentine Tierra del Fuego comprises part of the roughly east-west trending southern end of the Andean Cordillera intensely deformed since the Mesozoic. Mesostructures have been measured in Late Jurassic to Miocene rocks. Taking into account statistical criteria to provide a representative stress tensor from a fault population, this study defines 28 paleostress tensors pertaining to 22 sites. The orientation of σ_1 shows two main modes trending E-W to ESE-WNW and NE-SW. In addition, extensional sites reveal N-S, NE-SW, ESE-WNW, and NW-SE horizontal σ_3 and vertical σ_1. The stress fields obtained are congruous with a regional NE-SW compressive stress direction active in the study zone since the Late Cretaceous. Shortening was coeval with a 30° counterclockwise rotation of the Patagonian orogenic curve and the indentation of the orogenic wedge against a basement high, the Río Chico Arch, up to the early Miocene. The indentation caused a modification in the orientation of the compressive stress trajectories, showing NE-SW direction in Sorondo Range sector and NW-SE in Mitre Peninsula area. Since the late Miocene, left-lateral activity along the Magallanes-Fagnano Fault System produced local deviations of the NE-SW compressive stress toward an E-W direction. The present-day stress field is also characterized by NE-SW subhorizontal *P* axis derived from earthquake focal mechanisms and geodetic studies.

1. Introduction

Obtaining paleostress tensors of a determined region allows the stress field acting during a certain geological period to be analyzed (Bergerat & Vandycke, 1994; Eyal & Reches, 1983, among others). Yet stress field is heterogeneous at both the spatial and the temporal scale. If we assume that the stress field remains constant over a particular time interval, it is therefore necessary to provide a sufficiently large data set to be able to detect orientation variations at the regional scale. The variations may be related to diverse tectonic states over time or to the activity of large faults (Armijo et al., 1986; Casas & Maestro, 1996; Maestro et al., 2014; Maestro & López-Martínez, 2011; Simón, 1984, 1986; Tapponier & Molnar, 1976). The relationship between the activity of large faults and the deflection of stress trajectories has been studied through mathematical means and analog models (e.g., Casas et al., 1992, and references herein).

The Fuegian Andes, located in the southern end of the Andean Cordillera, also constitute the northwestern part of the Scotia Arc, which surround the Scotia and South Sandwich plates (Figure 1a). The geodynamic evolution of the Fuegian Andes is connected with the progression of the Scotia Arc, resulting in geological features that distinguish them from the rest of the Andean Cordillera. The external part of the orogenic chain is termed Fuegian thrust-and-fold belt (FTFB) with NW-SE, W-E, and WSW-ENE trends (Figure 1b). The FTFB involves Upper Jurassic-Lower Cretaceous sedimentary rocks deposited in the Rocas Verdes back-arc basin and in the Austral-Magallanes foreland basin during the Late Cretaceous-Neogene (e.g., Calderón et al., 2013). Sedimentary rocks were detached and imbricated along NE- to N-vergent thrusts (Torres Carbonell, Rodríguez Arias, & Atencio, 2017, and references therein; Figure 1c). A major left-lateral strike-slip fault system, the Magallanes-Fagnano fault deforms the FTFB (Klepeis, 1994; Tassone et al., 2005; Torres Carbonell et al., 2008; Figure 1b). This fault zone extends eastward along the North Scotia Ridge and represents the onshore expression of the left-lateral transcurrent boundary separating the Scotia and South American plates (Barker, 2001; Figure 1a). By analyzing brittle mesostructures, we were able to characterize a number of paleostress fields associated with these contrasting tectonic stages of the Fuegian Andes evolution.

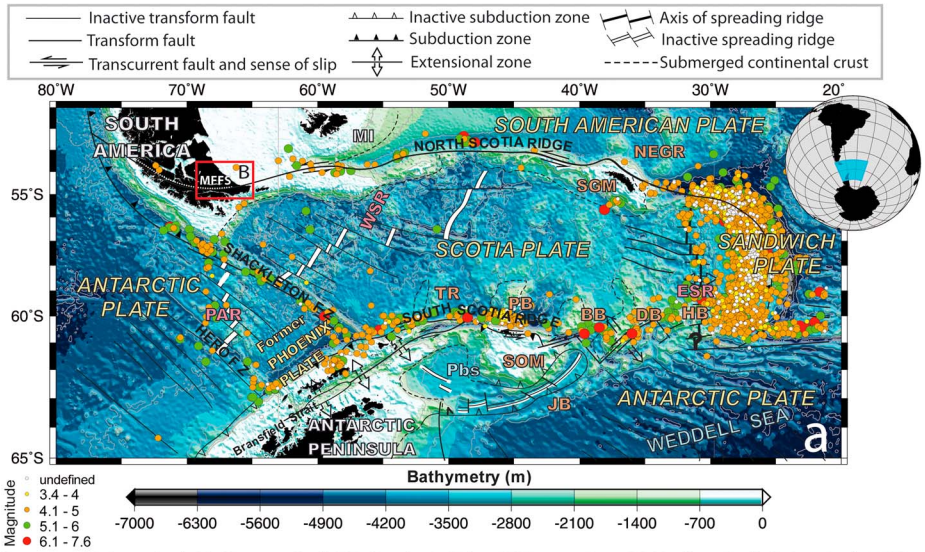

Toponyms: BB, Bruce Bank; DB, Discovery Bank; ESR, East Scotia Ridge; FZ, Fracture Zone; HB, Herdman Bank; JB, Jane Bank; MFFS, Magallanes-Fagnano Fault System; NEGR, Northeast Georgia Rise; PAR, Phoenix-Antarctic Ridge; PB, Pirie Bank; Pbs, Powell Basin; SGM, South Georgia Microcontinent; SOM, South Orkney Microcontinent; TR, Terror Rise; WSR, West Scotia Ridge.

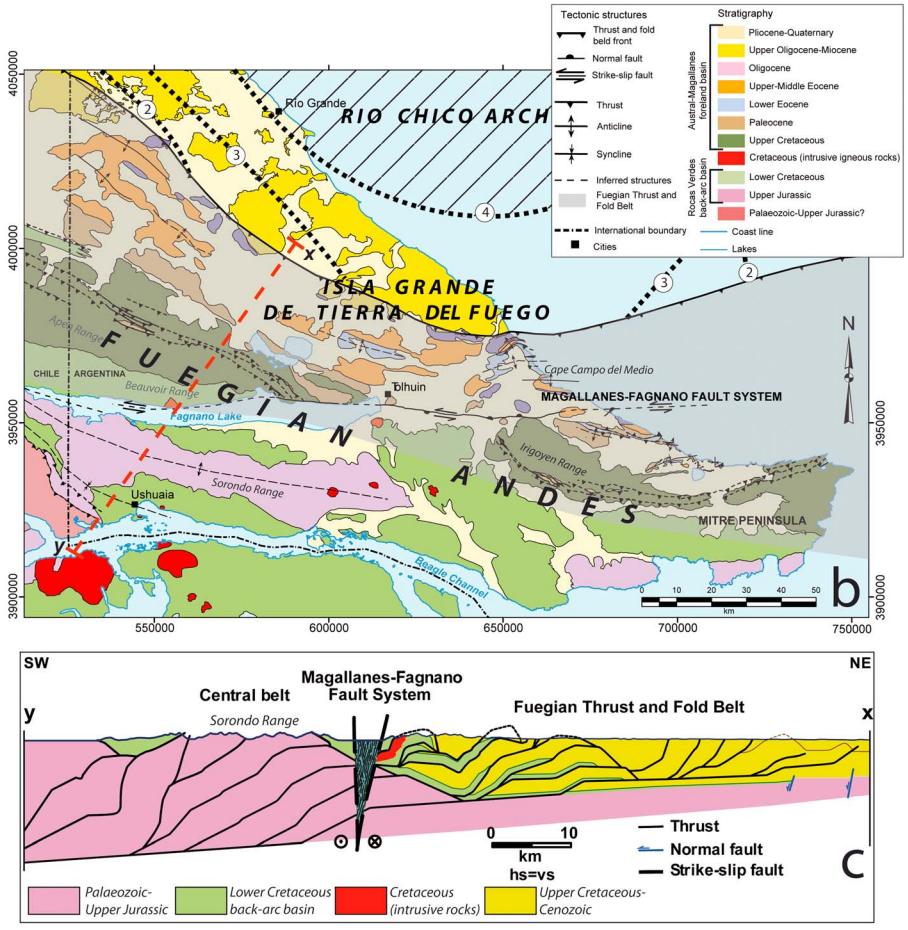

Figure 1. Situation of the study zone of the Argentine Tierra del Fuego in the Scotia Arc. (a) Tectonic and bathymetric map of northern Antarctic Peninsula and southern Scotia Arc regions (Galindo-Zaldívar et al., 2006). Bathymetric map has been carried out from satellite and ship track data (Smith & Sandwell, 1997). The study area is marked by a red box. Earthquake epicenters from National Earthquake Information Centre (USGS, 2013). (b) Simplified geological structural map of Argentine Tierra del Fuego (Olivero & Malumián, 2008; Torres Carbonell & Dimieri, 2013). Contours indicate foreland sediment thickness in kilometers (Biddle et al., 1986; Galeazzi, 1998). (c) Cross-section *x-y* of the Central Belt, the Magallanes-Fagnano Fault System, and the Fuegian Thrust and Fold Belt modified from Torres Carbonell, Cao, and Dimieri (2017).

The purpose of this investigation is (i) to characterize late Mesozoic and Cenozoic paleostress fields in the Fuegian Andes; (ii) to compare the obtained paleostress with the present-day stress pattern, deduced from focal mechanisms and GPS observations; and (iii) to determine the relationship between the evolution of the FTFB and the direction of the stress fields.

2. Geological Setting of Tierra del Fuego

The geological evolution of Tierra del Fuego can be divided for the purpose of this article into three major tectonic stages: (1) marine back-arc basin formation during Late Jurassic rifting and Early Cretaceous, (2) inversion of the back-arc basin during Late Cretaceous and propagation of contractional deformation to the foreland until the early Miocene, and (3) strike-slip regime linked to the left-lateral transform boundary between the major plates during and after the late Miocene (~10 Ma).

2.1. Back-Arc Basin Development

The first stage involved Late Jurassic continental stretching in the southwestern part of Gondwana that led to development of a rift and to accumulation of volcanic and volcanosedimentary units above Paleozoic rocks (Calderón et al., 2016, and references therein). Lithosphere-scale extension induced sea floor spreading in the Rocas Verdes back-arc basin (Dalziel et al., 1974, among others). Lower Cretaceous Flysch units derived from the arc filled the southern basin border, now preserved in Tierra del Fuego (Olivero & Martinioni, 2001; Figure 1b). The back-arc basin was at that time part of the continental connection between the Antarctic Peninsula and southern South America (e.g., Dalziel et al., 1975, among others). An important basement high located along the northeastern border of the basin, the Río Chico Arch, notably influenced the geometry of the future fold-and-thrust belt (e.g., Biddle et al., 1986; Figure 1b). Its subsurface topography was controlled by high-dipping normal faults of the Jurassic rifting (e.g., Robbiano et al., 1996).

2.2. Late Cretaceous-Miocene Basin Closure and Orogenic Growth

The second stage involving back-arc basin closure, tectonic emplacement of ophiolitic complexes, and underthrusting of the South American craton occurred at the beginning of the Late Cretaceous (e.g., Calderón et al., 2012, and reference herein). This process finally led to the collision of the volcanic arc against the craton (Klepeis et al., 2010; Nelson et al., 1980). The collision gave rise to stacking and duplexing in the upper crust connected to thin-skin shortening along the FTFB, deforming the sedimentary cover toward the foreland (e.g., Torres Carbonell & Dimieri, 2013; Figure 1c). Shales and fine-grained sedimentary successions of the back-arc basin act as detachment levels active during the establishment of the Austral-Magallanes foreland basin (Torres Carbonell, Rodríguez Arias, & Atencio, 2017, and references therein).

Paleomagnetic constraints derived from samples of Late Jurassic to Late Cretaceous rocks from the Fuegian Andes core suggest that the initial deformation of the orogenic wedge may have involved counterclockwise rotation of about 30° (Rapalini et al., 2015), whereas data from younger sediments suggest that rotation ceased after 60 to 50 Ma (Maffione et al., 2010; Poblete et al., 2014). Therefore, structural data and analog models also suggest that part of the orogenic curve, the Patagonian curve (or arc), may have formed at the onset of Late Cretaceous orogenesis (e.g., Ghiglione et al., 2016). The final curvature may reflect interaction of the FTFB advance with the Río Chico Arch, which exerted a major buttress along the Mitre Peninsula recess (Torres Carbonell et al., 2016; Figure 1b). At the apex of the recess, this final curvature involved some orthogonal flexure, as can be interpreted from N-S oriented folds that overprint middle Eocene structures (Torres Carbonell et al., 2016).

Ocean floor spreading in the Scotia plate and opening of the Drake Passage and the Western Scotia Sea after the middle Eocene highly condition the evolution of the orogen. The breakup entailed northward displacement of a major block formed by the magmatic arc and the incipient Fuegian Andes orogenic wedge. This block, coeval with the mentioned counterclockwise bending (e.g., Rapalini et al., 2015), pushed the back-arc and the synorogenic sequences of the foreland basin against the Río Chico Arch, until the early Miocene (Torres Carbonell et al., 2014).

2.3. Late Neogene Strike-Slip Tectonic Regime

During the third tectonic stage, the evolution of the Scotia Arc was further conditioned by the tectonic regime in the studied area. A left-lateral transcurrent boundary between the South American and Scotia

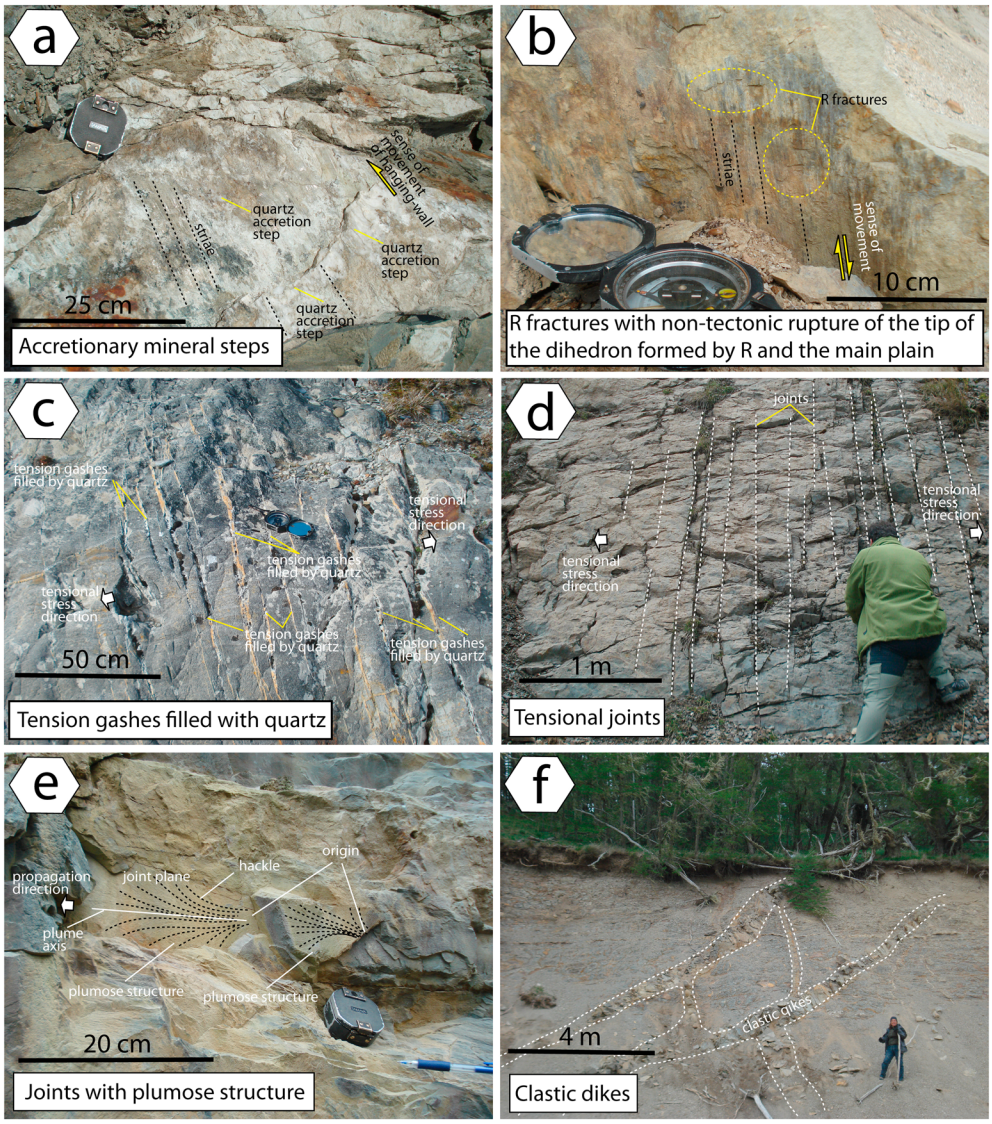

Figure 2. Examples of brittle mesostructure samples analyzed in this study.

plates developed along the North Scotia Ridge (Sue & Ghiglione, 2016, and references therein). This plate boundary is connected to the Magallanes-Fagnano fault system that cuts the FTFB and has generated a maximum left-lateral strike off-set of nearly 50 km and remains active (Bohoyo et al., 2007; Klepeis, 1994; Torres Carbonell et al., 2008; Figure 1a). This transcurrent plate boundary may have originated from a coincidence of (Barker, 2001) the following: (i) the cessation of eastward displacement in the North Scotia Ridge after collision of the East Georgia Rise with the South Georgia Microcontinent, (ii) the beginning of oceanic spreading in the East Scotia Ridge, and (iii) the interruption of seafloor spreading in the West Scotia Ridge.

3. Materials and Methods. The Palaeostress Database

We studied new 1,496 brittle mesostructures (1,236 faults, 113 joints, 67 tension gashes, and 64 clastic dikes) obtained from 87 sites in Early Jurassic-Late Cretaceous metamorphic and igneous rocks and Paleogene to Quaternary sedimentary rocks (Figure 2).

Fault data were analyzed with the Etchecopar (Etchecopar et al., 1981), y-R (Simón, 1986), Right Dihedra (Angelier & Mechler, 1977), Stress Inversion (Lisle et al., 2001; Reches, 1978), and Search Grid Inversion

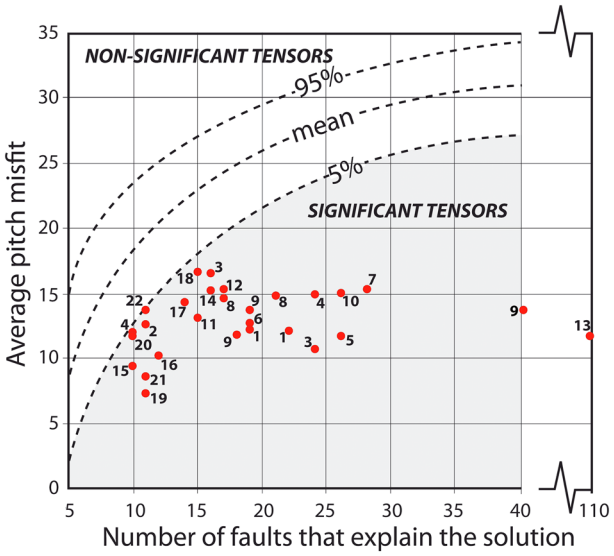

Figure 3. Representation of stress tensor solutions obtained from the fault population analysis used in this study (see Table S1 in the supporting information) on the significance diagram proposed by Orife and Lisle (2006).

Paleostress Determination (Galindo-Zaldívar & González-Lodeiro, 1988) methods. The use of different fault analysis methods guarantees the reliability of the obtained results. The paleostress results are mainly based on the fault population analysis; nevertheless, the orientations of joints, tension gashes, and clastic dikes are also useful as a complementary record of paleostress directions. There are numerous studies focused on the mechanical interpretation of joints as stress indicators (e.g., Engelder & Geiser, 1980; Hancock & Engelder, 1989). Tension and shear joints (e.g., Hancock, 1985) provide information of the maximum and minimum horizontal stress direction, but the estimation of the stress ratios cannot be established. Finally, the tension gashes and clastic dikes develop orthogonal to the minimum horizontal stress axis (Ramsay & Huber, 1983). Results are given with orientation of maximum (σ_1), intermediate (σ_2), and minimum (σ_3) stress axis. Furthermore, we indicate σ_y (azimuth of the maximum horizontal stress) and the value of R (stress ratio in Bott's equation; Bott, 1959), Rb = $(\sigma_z - \sigma_x)/(\sigma_y - \sigma_x)$, where σ_z is vertical and $\sigma_y > \sigma_x$ (see Table S1 in the supporting information). By plotting the poles of the joints, tension gashes, and clastic dikes planes, a representative minimum stress axis (σ_3) is obtained (see Table S2 in the supporting information).

The measured fractures are distributed in 87 stations, where the populations measured in each of them range between 1 and 109 data. Theoretically, only four faults are necessary to obtain stress tensors; nevertheless, this amount of data is not enough to derive a statistically representative solution. The minimum size of the fault population to establish the credibility or significance of the stress tensor solution obtained after the analysis has been widely discussed (e.g., Lacombe, 2012; Simón, 2018). Angelier (1979) and Etchecopar (1984) suggested using at least15 fault data; Casas et al. (1990) propose that this number could be lower and consider acceptable populations between 10 and 12 faults; in other cases, for example, in the case of nearly uniaxial stress regimes, Arlegui and Simón (1998) increases the number of data necessary for the solution to be acceptable to 25–30. Orife and Lisle (2006) establish a method to discriminate between significant and nonsignificant stress tensors. They take into account both the absolute number of faults that define the stress solution and the average misfit angle, and it is based on comparing with artificial solutions inverted from random data sets. In addition to these proposals, other authors (Delvaux et al., 1997; Simón et al., 2000; Sperner & Zweigel, 2010) have attempted to establish a categorization of stress tensor solutions based on a series of parameters that classify them from excellent to unacceptable solutions. In general, the main criteria used in such evaluation are the degree of directional dispersion of the results, the proportion of explained faults respect to the full population, and the mechanical compatibility of fault orientations with the obtained stress tensor. We have thought that it is more appropriate to establish a clear differentiation between acceptable and unacceptable solutions than to classify the solutions according to their quality, for that reason we have used the separation between significant and nonsignificant solutions proposed by Orife and Lisle (2006) to eliminate the most debatable solutions. We have plotted our solutions on the diagram of significance proposed by these authors where the representation shows the average pitch misfit versus the number of faults that explain the solution (Figure 3). The 5% curve determines the boundary between significant (less than 5% of probability of being spurious solutions resulting from a random combination of fault-slip data) and nonsignificant stress tensors. It has also been taken into account, as proposed by the authors, that this quality indicator is not very useful when considering solutions defined from a population of less than 10 samples. Finally, we have only considered as significant solutions in this study 28 paleostress tensors pertaining to 22 sites (see Figure 3). The equal area and lower hemisphere projections with the orientation of faults and slickenside striations data of the sites with significant stress tensors is showed in Figure S1 in the supporting information.

The stress tensors, as well as the compression and tensional directions, are represented using two types of graphics. The spherical projections projection of σ_1, σ_3, and σ_y axes of the stress tensors obtained from fault-slip data samples, joints, tension gashes, and clastic dikes are shown in Figures 4a–4c. In addition, a two-coordinate diagram shows the relationship between the azimuth of the maximum horizontal

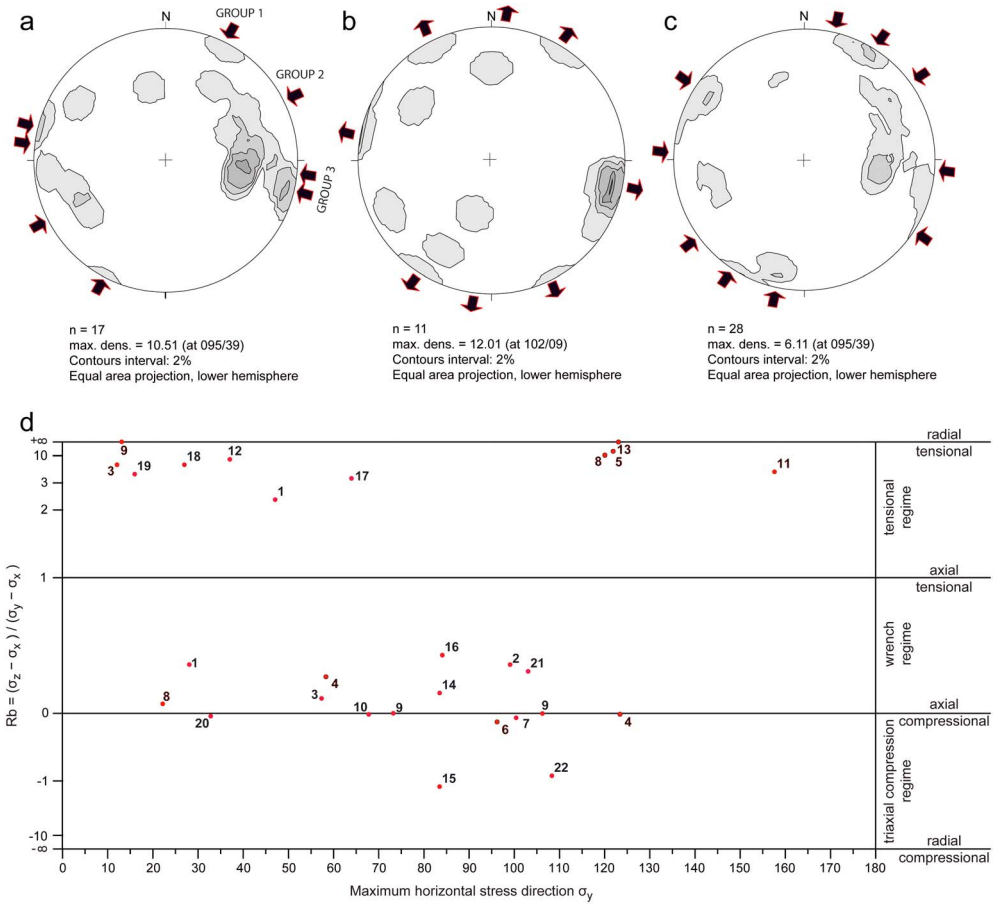

Figure 4. Density equal area, lower hemisphere projections, and contour interval 1% representing (a) compression (σ_1), (b) extension (σ_3), and (c) greatest horizontal stress (σ_y) axes obtained from the analysis of brittle mesostructures. (d) y-R diagram showing all the stress tensors obtained in Tierra del Fuego (see Table S1 in the supporting information). σ_y is the azimuth of the major horizontal axis; Rb = $(\sigma_z - \sigma_x)/(\sigma_y - \sigma_x)$, where σ_z is vertical and $\sigma_y > \sigma_x$ (Bott, 1959). The stress regimes corresponding to the different values of the stress ellipsoid shape ratio are indicated at the right of the graph.

stress (σ_y) and the shape ratio of the stress ellipsoid (Rb; Figure 4d). The latter representation only shows the stress tensors assuming one of their axes to be vertical; otherwise, the axis that approaches the vertical is regarded as vertical for plotting the stress tensor. This representation resembles the graphics of the y-R method (Simón, 1986).

The present-day stress orientation has been established from the analysis of the earthquake focal mechanism data (see Table S3 in the supporting information) and even geodetic measurements. There are numerous studies that use the focal mechanisms to establish the recent stress field (e.g., Zoback, 1992; Müller et al., 1992; Heidbach et al., 2007, 2010; Olaiz et al., 2009; Lund Snee & Zoback, 2016). Lacombe (2012) compares a couple of studies that relate paleostresses obtained from the fault population analysis by stress inversion methods with modern stresses (earthquake focal mechanisms and breakouts) and geodetic measurements, observing a high level of congruence between them. This author considers that their joint use of paleostress orientations from fault slip data and recent stress orientations can be an important contribution to establish the reliability of the reconstruction of paleostresses in areas where the stress orientations have remained stable with time. The focal mechanisms data were analyzed using the 'exact method' of FSMI software (Gephart, 1990) based on Gephart and Forsyth (1984). This method applies a search grid to determine a single stress tensor (three main axes and axial ratio, $R = (\sigma_2 - \sigma_3)/(\sigma_1 - \sigma_3)$; if $\sigma_1 = \sigma_z$, Rb = $1/R$; if $\sigma_2 = \sigma_z$, Rb = R; and if $\sigma_3 = \sigma_z$, Rb = $R/(R - 1)$) that is responsible for the focal mechanisms in regions affected by a homogeneous geological structure. It analyzes the orientations of fault planes and slip directions indicated by a population of earthquake focal mechanisms using inverse techniques similar to those used for calculating the stress

tensor from field observations of the orientation of striations on exposed fault surfaces. On the other hand, it is necessary to take into account the magnitudes of the earthquakes to establish possible uncertainties in the estimation of the focal mechanism. These uncertainties could occur in focal mechanisms obtained from earthquakes of small magnitude (Mw $<$ 5). Mooney (1989) considers for earthquakes with magnitude greater than 5 (earthquakes of moderate-high magnitude) that have been recorded since the mid-1960s, which a reliable focal mechanism can be obtained. In this study, the focal mechanisms considered are earthquakes produced from 1970 to 2015 and the Mw values are mostly greater than 5 (98%: 33% are Mw $\geq$ 5, 53% are Mw $\geq$ 6 and 12% are Mw $\geq$ 7, see Table S3 in the supporting information). Therefore, we consider that the data of the earthquakes focal mechanisms used in our study are of sufficient quality and confidence, making not necessary to weigh each focal solution according to its magnitude.

4. Mesozoic-Cenozoic Stress Fields From Brittle Mesostructure Analysis

Analysis of the measured fault orientations in Mesozoic and Cenozoic rocks shows a maximum striking NE-SW, and an ESE-WNW secondary direction, with modal dips between 65° and 80°. From the total population, 208 dextral strike-slip, 182 sinistral strike-slip, 275 reverse, and 571 normal faults were identified. The dextral strike-slip faults show two main orientations ENE-WSW and E-W, and a N-S secondary direction, with a modal dip of 85°. The sinistral strike-slip faults show three main directions NE-SW, ENE-WSW, and N-S, with a modal dip of 85°. The reverse faults show two maxima striking ESE-WNW and NNE-SSW, with a modal dip of 80°. The normal fault planes show a NE-SW main strike, with a modal dip angle of 65° and ENE-WSW to E-W secondary orientations.

The joint data set shows four relative maxima with N-S, NE-SW, ENE-WSW, and NW-SE orientations. The tension gashes show N-S and NE-SW orientation and thicknesses ranging from millimeters to centimeters. Most joints and tension gashes have vertical planes. The clastic dikes have a maximum trending NE-SW to ENE-WSW. Most clastic dikes show dips from 70° to subvertical and an average thickness of 35 cm.

The significant stress tensors show a relative maximum of compression direction E-W to ESE-WNW, with Rb relationships varying between wrench (55% of the tensors with E-W to ESE-WNW direction) to triaxial compressional regimes (45% of the tensors with E-W to ESE-WNW direction), but being close to an axial compressional regime (27% of the tensors with E-W to ESE-WNW direction). There is another relative maximum compression with NE-SW orientation, the stress tensors having Rb relationships within a wrench regime (50% of the tensors with NE-SW direction) close to an axial compressional regime (50% of the tensors with NE-SW direction; Figures 4a and 4d). There is also a relative maximum of σ_1 direction NNW-SSE to NNE-SSW, with Rb values within the wrench regime (Figures 4a and 4d). The orientation of σ_3 shows two main modes trending N-S, NE-SW, ESE-WNW, and NW-SE, with Rb relationships within a tensional regime (82% of the tensors) tending to radial tensional regime (18% of the tensors; Figures 4b and d). σ_y orientations show a ESE-WNW main trend and three secondary modes with NE-SW, NNE-SSW, and NW-SE directions (Figure 4c).

4.1. Spatial Distribution of the Compression Directions

The compression directions (Figure 5a) derived from fault population analysis can be grouped in sets, considering their location and their relationship with existing geological structures:

1. The NNW-SSW to NNE-SSW compressional stress direction is located in the Late Jurassic-Early Cretaceous rocks of Sorondo Range (sites 1 and 8), oblique to the structural trend of the area (NW-SE to WNW-ESE direction).
2. The NE-SW compressional stress direction was determined in two sites in the southwestward of Argentine Tierra del Fuego, located in the Late Jurassic and Early Cretaceous rocks (sites 3, 4, and 10). In these sites they are perpendicular to the macrostructures, mainly thrusts and large folds. NE-SW stress compression is also found in the Eocene rocks of the northern part of Mitre Peninsula (site 20), oblique to the structural trend showing a ENE-WSW direction.
3. In general, the E-W to ESE-WNW stress compressional direction is arranged oblique to the direction of the main macrostructures, as seen in the Late Jurassic to Late Cretaceous rocks of Sorondo range and Paleocene rocks NE of Apen range, in one near Cape Campo del Medio and in the north of the Mitre Peninsula (sites 4, 9, 21, and 22). On the other hand, in Apen and Irigoyen ranges (sites 14 and 15), the E-W compressional stress is perpendicular to the thrusts that affect the Upper Cretaceous-

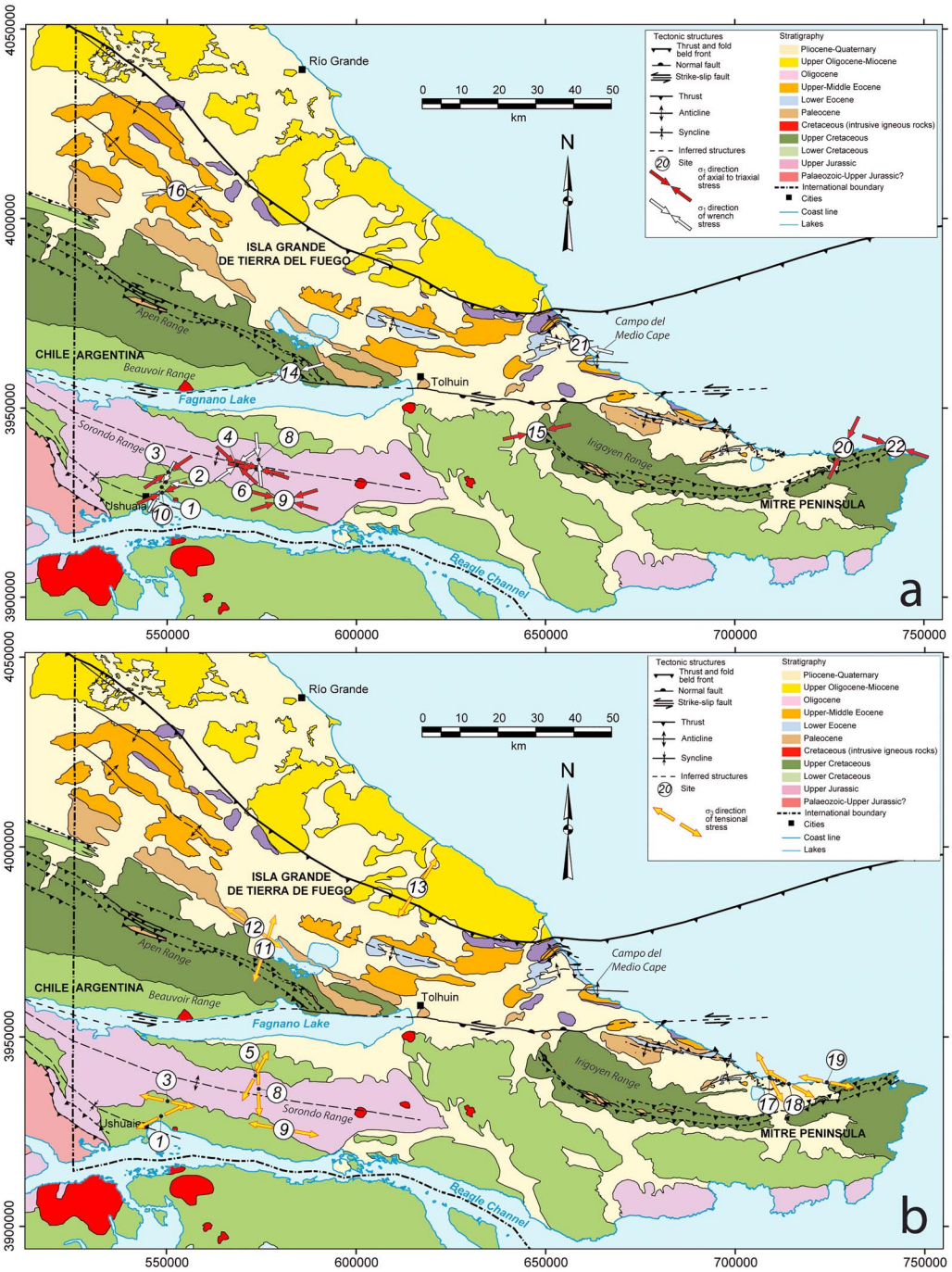

Figure 5. Geological maps of the studied area with location of study sites having (a) compressional and wrench stress tensor results and (b) tensional stress tensor results.

Paleocene units. Finally, the E-W stress direction is arranged parallel to major fold axes in Sorondo Range (sites 6, 7, and 9).

4.2. Spatial Distribution of the Tensional Directions

It is possible to establish some generalizations of the stress tensors with horizontal σ_3 and vertical σ_1 regarding their spatial distribution and their relationship with the tectonic macrostructures (Figure 5b):

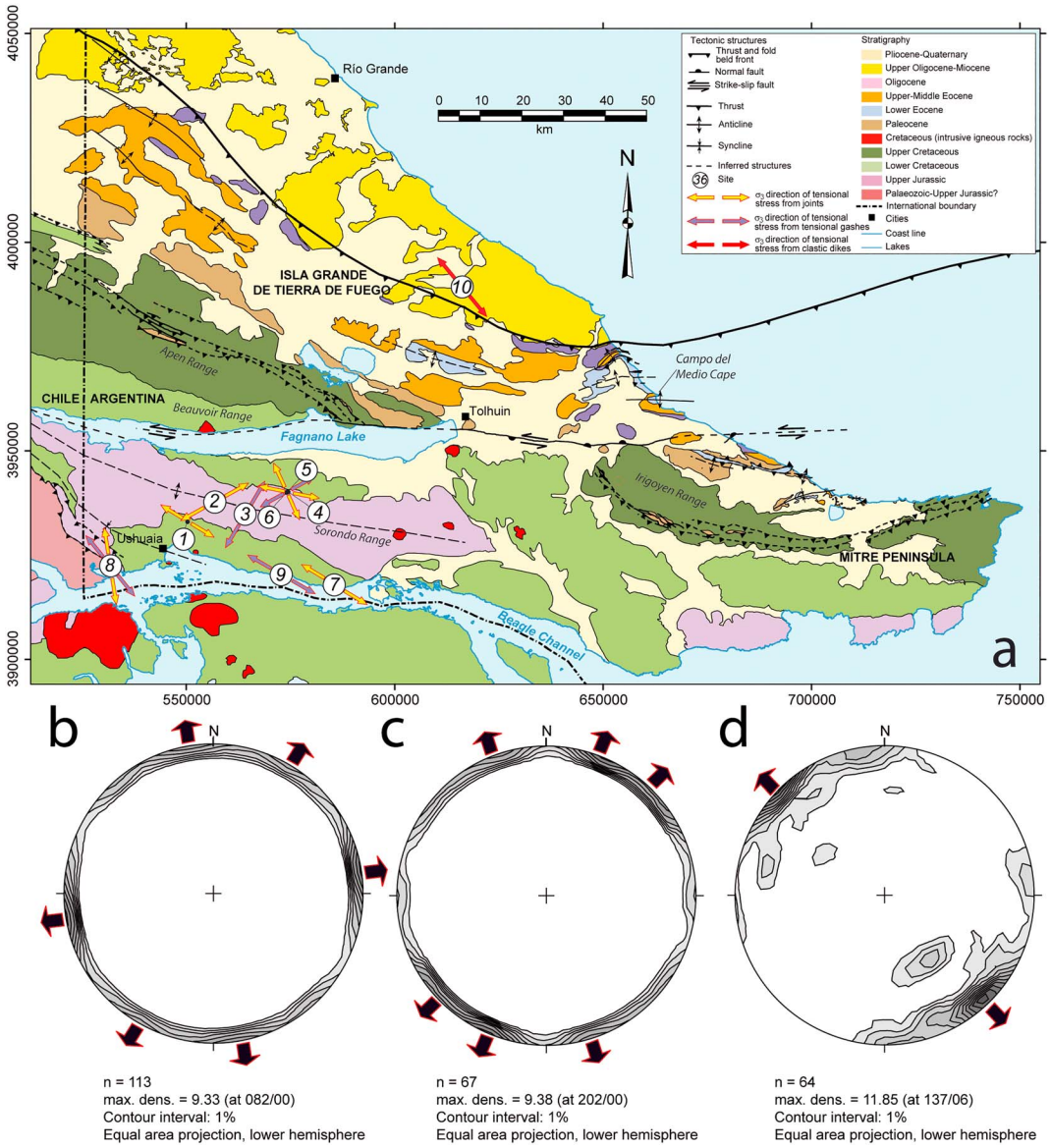

Figure 6. (a) Geological maps of the studied area and location of study sites with tensional stress tensor results obtained from population analysis of joints, tension gashes, and clastic dikes (see Table S2). Density equal area, lower hemisphere projections, and contour interval 1%, representing plane poles of joints (b), tension gashes (c), and clastic dikes (d).

1. There is a N-S tensional direction in a site located in the Upper Jurassic rocks of Sorondo Range (site 8) and in the Upper Cretaceous rocks of Apen Range (site 11). Such σ_3 directions are subperpendicular to the traces of thrusts, folds, and the Magallanes-Fagnano Fault System.
2. The site with NE-SW σ_3 direction tensors is also located in Sorondo Range. This direction of stress tensors is arranged perpendicular (site 5) to the trace of the main geological structure mapped.
3. There are two sites that show an ESE-WNW stress tensional direction. They are located in Sorondo Range and in the northern part of Mitre Peninsula. These are arranged parallel to the direction of the macrostructure map traces (sites 3 and 19).
4. The sites that show tensional tensors with NW-SE direction are also mainly located in Apen Range and in the northern part of Mitre Peninsula. These tensors are arranged parallel (site 12) and perpendicular (sites17 and 18) to the direction of the traces of thrusts and folds.
5. Two sites show tensional stress tensors with Rb relationships within a radial tensional regime (sites 16 and 20).

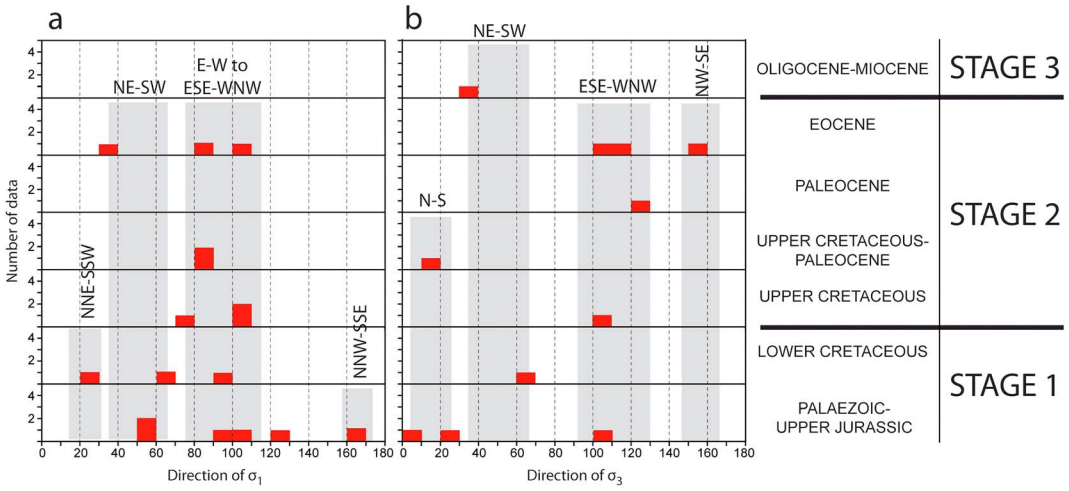

Figure 7. Relationship between directions obtained from brittle mesostructures, and the age of geological units in which they are recorded: (a) compressional stress directions (σ_1) and b extensional stress directions (σ_3) only from extensional tensors.

6. One site shows the direction of the compressive stress tensor and the tensional stress tensors with similar orientation patterns (site 8).

The tensional brittle mesostructures (tension gashes, joints, and clastic dikes) are mainly detected in the southwestern part of the study zone (see Figure 6). From σ_3 orientations, a main NW-SE tensional direction is observed. There is also a relative maxima of σ_3 directions NE-SW. The principal axes of these tensors are arranged parallel (sites 1, 4, 7, 8, 9, and 10), perpendicular (site 3), and oblique (sites 2, 5, 6, and 8) to the trace of the main tectonic structures mapped (Figure 6a).

4.3. Chronology of the Stress Tensors

In general, it is very difficult to determine the age of the obtained stress tensors. In our case we do not have the cross-cutting relationships between superposed striae on one fault plane, so the only criterion that gives us information about the relative age of the tensors is the depositional age of the rocks affected by the measured mesostructures, which gives a maximum age. Moreover, the uniformity in the distribution of some tensor orientations in rocks of different age makes possible a first approximation to constrain the span for the related stress field.

The small number of significant tensors obtained in the study area means that any approach to establish the age of the tensors has a certain degree of speculation. In spite of this, taking into account the above premise, we can establish a series of time intervals in which the different directions of both compressional and extensional tensors have acted in a preeminent way. Then, taking into account the age of the rock units affected by the faults, we could interpret that the NNE-SSW and NNW-SSE compression are not recorded in rocks younger than the Lower Cretaceous and NE-SE and E-W to ESE-WNW σ_1 are recorded at least until the Eocene, which is the youngest age of the rock units in which faults have been measured (Figure 7a). On the other hand, the N-S minimum stresses are not recorded in rocks younger than Upper Cretaceous to Paleocene and NE-SW, ESE-WNW, and NW-SE σ_3 are present at least until the Eocene to Miocene (Figure 7b).

5. Discussion

We compared the interpreted chronology of the obtained stress tensors (see above), with the known geodynamic history of southernmost South America, as established in previous research. The following discussion, therefore, puts forward a model to explain how the stress fields evolved during the evolution of the southernmost Andean Cordillera, which honors both our data and previous tectonic models.

5.1. Mesozoic to Cenozoic Compressive Stress Field

The closure of the Rocas Verdes back-arc basin started in the beginning of the Late Cretaceous due to the rapid westward motion of the South American Plate relative to a mantle reference frame, enhancing compression along the western boundary of South America (Dalziel, 1986). During the closure of the basin, obduction of the oceanic crust and underthrusting of the South American continental margin took place (Calderón et al., 2012; Klepeis et al., 2010; Nelson et al., 1980), ending with the collision of the South American continental margin with the magmatic arc that rimmed the Rocas Verdes basin on its Pacific sector (Cunningham, 1995; Klepeis et al., 2010; Maloney et al., 2011; Nelson et al., 1980). This produced large-scale folding and thrusting of the continental margin (Klepeis et al., 2010; Torres Carbonell & Dimieri, 2013). Subduction of the former Phoenix Plate below the Pacific-side arc continued coeval with closure and collision (Mukasa & Dalziel, 1996).

In our schematic model (Figure 8), we interpret that this orogenesis started under a compressional stress regime with NE-SW direction, caused by the tectonic underthrusting within the closing Rocas Verdes basin. Progression of deformation resulted in the development of the mesoscale fractures when the rocks in the Fuegian Andes were already subjected to an initial stage of ductile deformation and partial uplift, which favored the development of brittle structures (Figures 8a and 8b). In this context, the collision of the magmatic arc involved up to 30° counterclockwise rotation which, in the deformed Rocas Verdes basin rocks (Rapalini et al., 2015). Likewise, Poblete et al. (2016) show paleomagnetic results obtained from Cretaceous to Eocene rocks that indicate counterclockwise rotations varying from ~30° to more than 90° in the magmatic arc (Fuegian backstop). In our study area, rotation of the orogenic wedge is younger than ~70 and older than~50 Ma (Maffione et al., 2010; Rapalini et al., 2015).

The regional counterclockwise rotation accordingly developed a progressive arc structure related to the folding with vertical axis of the fold-and-thrust structures, the original NW trend acquiring a WNW to E-W orientation (Poblete et al., 2016; Torres Carbonell et al., 2014). This process rotated the successively forming mesofracture sets, which therefore indicate rotated paleostress tensors (e.g., NE-SW to N-S; Figures 7a and 7b). It also implies a replacement of the regional NE-SW compression by a local NNW-SSE to NNE-SSW compression due to the push of the rotating magmatic arc on the foreland sequences, eventually incorporated into the orogenic front. This effect can be locally seen from the orientation of σ_1 derived from the Stage 1 disjunctive foliations in the Late Cretaceous paleo-orogenic front (cf. Torres Carbonell et al., 2013; Figure 8a). The consequence of a rotating backstop on changing contraction directions along the belt has also been reproduced using analog models with a tectonic configuration almost identical to that of the Fuegian Andes (Torres Carbonell et al., 2016).

The FTFB propagation toward the foreland during the Late Cretaceous to early Neogene was hindered the buttressing effect of a notable basement promontory called the Río Chico Arch (Torres Carbonell et al., 2016; Torres Carbonell, Rodríguez Arias, & Atencio, 2017). This promontory was located in the NE border of the Rocas Verdes basin and was inherited from the Late Jurassic rifting stage (Biddle et al., 1986; Yrigoyen, 1989). There is a rough coincidence of the southern border of the Río Chico Arch with the FTFB front in eastern Tierra del Fuego (Mitre Peninsula). The effect of the interaction between the Río Chico Arch and the FTFB propagation was registered in the stress field variation observed in the studied area (Figure 8b): the western area of the study zone shows a NE-SW dominant orientation of the σ_1, and in the northern sector of Mitre Peninsula, coinciding with the southern border of the Rio Chico Arch, the stress tensor obtained from the fault population analysis shows a main NW-SE orientation for the average maximum compressive direction (Figure 8b). Deformation in the FTFB continued until the Miocene through the northward propagation of thrust sheets that molded the Río Chico promontory (Ghiglione et al., 2010; Ponce et al., 2008; Torres Carbonell, Rodríguez Arias, & Atencio, 2017).

5.2. Late Neogene Strike-Slip Stress Field

Regional neogene strike-slip faulting in the Fuegian Andes is related to creation of the sinistral transform fault that bounds the Scotia Plate to the north. In Tierra del Fuego this regime is manifested by the Magallanes-Fagnano Fault System, with a strike separation of ~50 km imposed on the FTFB (Torres Carbonell et al., 2008). This transcurrent fault shows in some segments, a normal component with a vertical displacement below 3 km (Klepeis, 1994). Taking the geodetic slip rates established for this fault by Smalley et al. (2003)

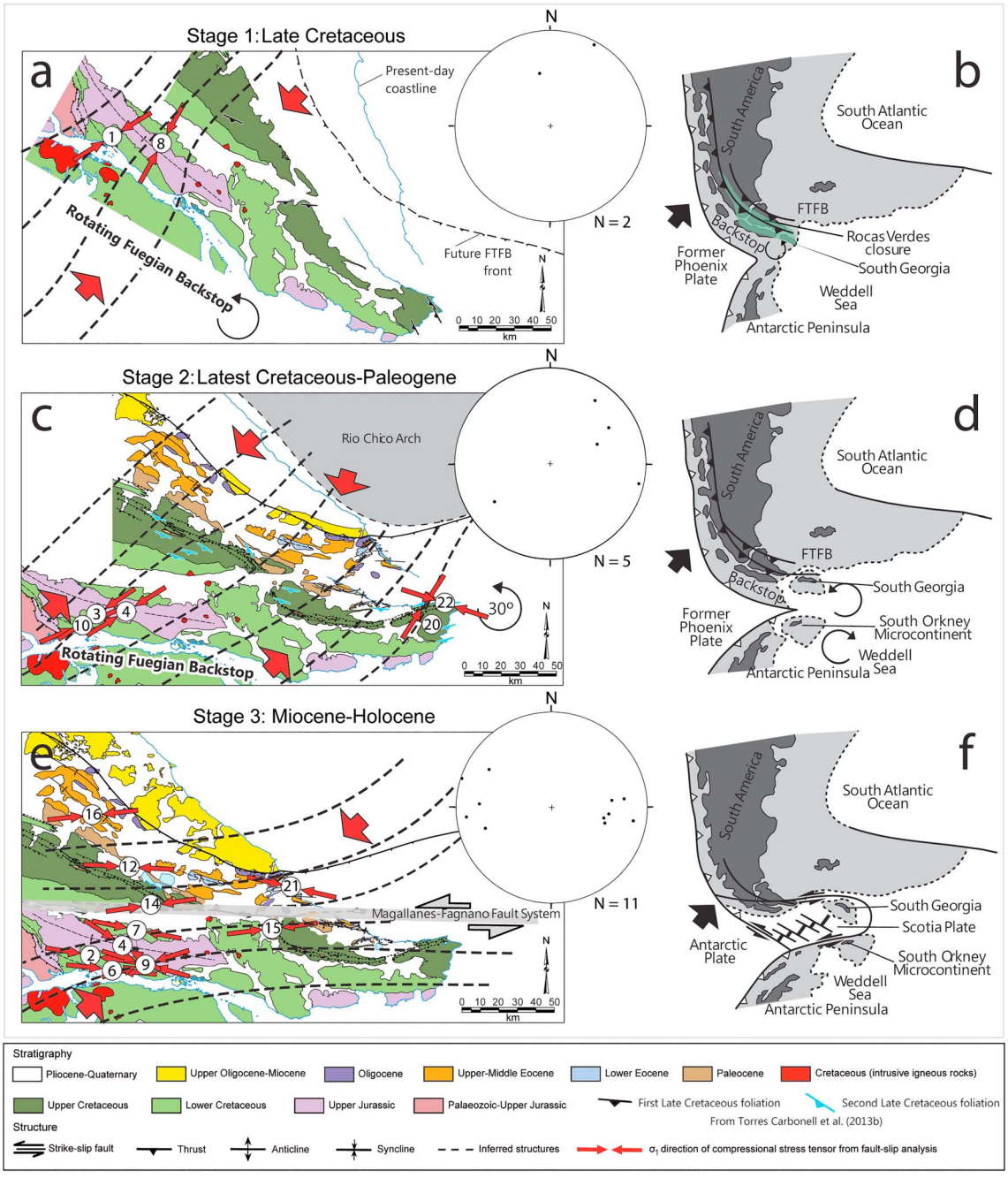

Figure 8. Stress field evolution of Argentine Tierra del Fuego and geodynamic evolution of the Fuegian Andes and the Antarctic Peninsula from Late Cretaceous until Quaternary (Stage 1 to Stage 3). Lines with white and black triangles are subduction and thrust zones, respectively. The curved arrows indicate rotations of crustal blocks, the small red arrows show σ_1 direction of compressional stress tensor from fault-slip analysis, the large red arrows show remote shortening directions' driven by plate kinematics, and black arrows show subduction direction. Equal-area lower hemisphere spherical projections include the compressional stress axes obtained from the fault population analysis related with the different stress field evolutionary stages established in this study. Schemes of the right part are modified from Diraison et al. (2000).

and Mendoza et al. (2011), which are about 6.6 ± 1.3 to 4.4 ± 0.6 mm/a, the strike-slip faulting would have started in the Late Miocene, between ~7 and ~11 Ma (Torres Carbonell et al., 2008).

This age is in accordance with the initiation of the sinistral regime along the South Scotia Ridge (Bohoyo et al., 2007). Bohoyo et al. (2007) propose that the oceanic spreading of the southern Scotia basins, between late Oligocene and middle Miocene, must have formed in a dextral strike-slip tectonic regime of the South

Scotia Ridge in relation to the eastward movement of the continental blocks. The East Scotia Ridge was characterized by asymmetric spreading from the middle Miocene to ~10 Ma, when the central part of the South Sandwich Arc was affected by a ridge jump and the western edge of the East Scotia Ridge was affected by slow spreading until ~6.5 Ma (Larter et al., 2003). On the other hand, the Shackleton Fracture Zone in the western border of the Scotia Arc acted as a purely oceanic transform fault until spreading ceased in the West Scotia Ridge at 6.5 Ma (Maldonado et al., 2000) and the Antarctic-Phoenix Ridge at 3.3 Ma. Synchronous with a decrease in the West Scotia Ridge oceanic spreading, the Shackleton Fracture Zone began to uplift 8 Ma ago. This amount of tectonic processes occurring since 8 Ma ago along the Scotia-Antarctic plates edge has been related to the stratigraphy of mass-transport deposits in the region by Pérez et al. (2016).

Surface ruptures along the Magallanes-Fagnano Fault System form an E-W ~10-km wide zone (Lodolo et al., 2003; Pedrera et al., 2014; Sue & Ghiglione, 2016; Torres Carbonell et al., 2008). Strike-slip and oblique faults in some scattered outcrops reveal kinematics consistent with regional sinistral strike-slip tectonics, everywhere postdating the compressive structures of the FTFB (Klepeis, 1994; Torres Carbonell et al., 2008, 2014).

The sinistral movement of the fault system is congruent with a regional NE-SW late Miocene compressive stress field. Deviations of its trajectory occur in the Magallanes-Fagnano Fault System, as seen in some sites situated near to the fault zone in the northern and southern blocks; the tensors obtained in this work can be interpreted as the deflected stress trajectories due to displacement of the fault system (Figure 8c). In general, mathematical models show how trajectories tend to be parallel to the fracture plane at the tips toward which the block moves and tend to be perpendicular to the opposite tips. The study area is located in the central segment of a large fracture zone that extends westward to the subduction zone of the Pacific Plate under the South American Plate and to the east extends far along of the North Scotia Ridge (see Figure 1). Therefore, we can underestimate the anchoring effect at the fault tips and attend to how the stress field deflection occurs in the central zones of the faults. Regarding this, there are numerous studies based on mathematical models and data obtained from the fault populations analysis and breakout wells (e.g., Aleksandroski et al., 1992; Homberg et al., 1997, 2004; Reynolds et al., 2005; Yale et al., 1994). The 2-D modeling of these studies shows that the orientation of the local stress perturbation closely parallels the fault orientation along the midsection of the fault in situations where there is a small angle between the maximum horizontal compressive stress orientation and the fault. Tingay et al. (2006) moreover considers the deflection processes of the stress field near geological structures to result from structures acting as a mechanical discontinuity. They consider that an *open* or very *weak* fracture in the subsurface will act as a free surface and be unable to sustain shear stresses. As a result, the stress field must be locally reoriented in the vicinity of the fracture so that one principal stress acts perpendicular to the fracture. Similarly, stresses will be locally deflected or *refracted* near the boundary between mechanical contrasts. In general, it is predicted that the maximum horizontal stress orientation will be deflected subparallel to mechanically weak structures. In the southern and northern blocks of the Magallanes-Fagnano Fault System, stress trajectories change from NE-SW to E-W direction near the fault zone. This agrees not only with a sinistral movement of the central part of the Magallanes-Fagnano Fault System but also with the NE-SW regional main compressive direction.

5.3. Tensional Stress Field: Local Vs. Regional Interpretation

In order to interpret the significance of the obtained extensional stress tensors, it is necessary first to constrain their relative age with respect to the geodynamic evolution of Tierra del Fuego during the Mesozoic and the Cenozoic. In that sense, we highlight that many of the faults that explain the tensional tensors appear to postdate the contractional structures of the Fuegian Andes; these cases the maximum compressive direction is almost vertical, suggesting that no major titling of the tensional tensor due to folding occurred. In fact, it has been possible to determine, from the existence of some fault planes with superposed striae, that the tensors with σ_1 in the horizontal are prior to the tensors with σ_3 in the horizontal and σ_1 in the vertical. It is difficult to confirm the relationship between tensors and major structures in the field, given that the folds in the thrust-fold belt are of large wavelengths (a few kilometers), thus exceeding the scale to which one could constrain timing of the small scale fractures studied in our work. However, we can argue that there are no major extensional tectonic features of an age pertaining to the late Cretaceous-early Miocene evolution of the thrust-fold belt (e.g., Torres Carbonell & Dimieri, 2013; Torres Carbonell, Rodríguez Arias, & Atencio, 2017). Therefore, it is more probable that the tensional tensors formed after the contractional structures, or even simultaneously with them, as explained in (2) below.

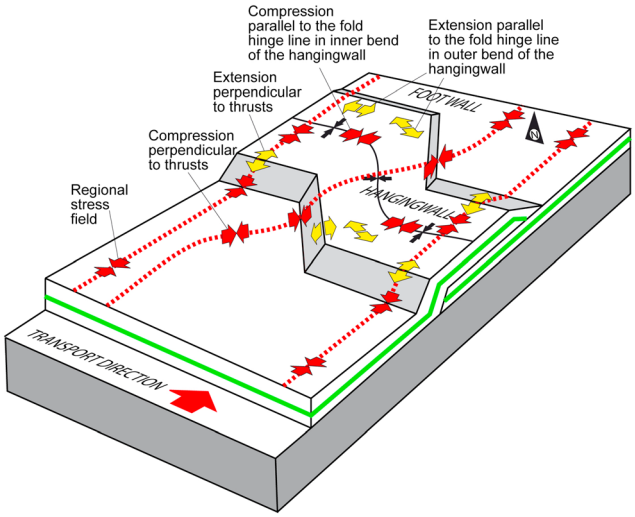

Figure 9. Block diagram showing the relationships between stress directions and a thrust fault with a fault bend fold in the hangingwall and footwall.

In this context, we consider that there are two possible explanations for the tensional stress tensors:

1. That these tensional tensors pertain to the episode of late Cenozoic regional uplift in Tierra del Fuego and southern Patagonia, which is independently constrained by few apatite fission track ages as young as 9 Ma in Cordillera Darwin (Nelson, 1982), positive dynamic topography for the last 10 Ma in the region (Dávila et al., 2018), and an important Holocene uplift due to isostatic rebound and/or recent tectonics after the last glacial maximum (Gordillo et al., 1992; Ivins & James, 2004; Mendoza et al., 2011). In the case of recent tectonics, the uplift may be related to local deformation related to the Magallanes-Fagnano fault system. The late Cenozoic uplift could have caused some extent of collapse of the mountain belt through extensional deformation, explaining the tensional and radial tensional regimes existing in some places (sites 9 and 13).
2. Overall, the extensional tensor trajectories from many sites are very alike the pattern of σ_1 trajectories. In these cases both parallel and orthogonal relationships are seen between folds-thrusts and σ_3 directions. The similarity between the orientation of the compressional and extensional directions can be explained considering the interaction between the orientation of the regional stress field and the kinematics of thrusts and associated folds. Extension perpendicular to fault-bend folds is known to be accommodated by external hinge faults (Figure 9) and has been described in the context of sequential compression and extension parallel to the transport direction in the associated thrust (Cooper, 1992; Turner & Hancock, 1989; Wojtal & Pershing, 1991). Conversely, slip on arcuate thrusts is known to cause extension parallel to the thrust-strike due to flexure of the convex hanging wall (Figure 9; Geiser, 1988; Marshak et al., 1992; Martínez-Peña et al., 1995).

There are several studies that show many examples of extension processes within folds (e.g., Cosgrove & Ameen, 2000; Lemiszki et al., 1994; Srivastava & Engelder, 1990). Normal faults formed in association with bend folding may be the result of local stresses generated due to extension in the external arc. The relationship between extensional structures—normal faults, joints and tension gashes—and fold geometry is usually quite simple. The local stress perturbations generated as a result of bending could produce an interchange of the principal stress axes that in turn causes these extensional structures to originate both parallel and perpendicular to the fold axis. Similarly, thrust faults form in the hinge regions below the inner arc of the fold, in the area of localized compression. The development of normal and/or thrust faults in the hinge region is controlled by the effective thickness of the layer which, in turn, may cause the migration of the neutral surface either up or down.

Thus, a second possibility is that the tensional stresses recorded are related to local stress perturbations associated to the development of folds in the thrust-fold belt (Figure 9). This is consistent with the lack of first-order extensional tectonic features in the thrust fold belt and would limit the tensional tensors not to regional stress fields but to local conditions. Furthermore, it is not unusual to find in the same site or in very close sites in rocks of the same age, superposed tensors where the compressive stress direction (σ_1) of one phase is arranged subparallel to the extensional stress direction σ_3 of the other (see Figure 5). For example, between sites 1 and 10 and in stations 8 and 9, it is possible to observe the marked parallelism that exists between the compressive (σ_1) and extensional (σ_3) stress orientations, with N-S, NE-SW, and E-W directions, with an average angular variation of 4° between them (Figure 5). This would corroborate that an important number of the extensional stress directions determined from the fault population analysis could correspond to local deformations linked to the development of folds and thrusts.

5.4. Recent and Present-Day Stress Field

The present-day stress field in Tierra del Fuego can be obtained with earthquake focal mechanisms (Table S3 in the supporting information). An approximately regional NE-SW compression in the region is suggested by the World Stress Map (Heidbach et al., 2007) from the U.S. Geological Survey National Earthquake Information Centre (United States Geological Survey (USGS), 2013) and the Harvard Seismology Centroid Moment Tensor

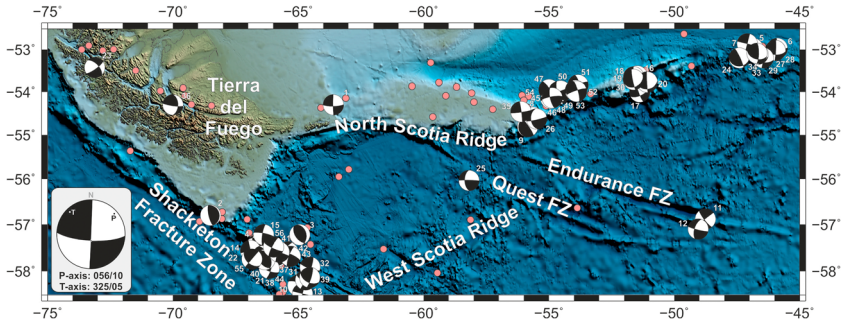

Figure 10. Present-day stresses from earthquake focal mechanism solutions in the study region derived from different sources (see Table S3 in the supporting information). Mechanism solutions are plotted as lower hemisphere equal-area projection, white quadrants indicating compressional *P* wave. Seismicity of magnitude greater than 5 Mw from National Earthquake Information Centre database is represented by red circles. Inset with the regional focal mechanism solution derived from the integration of all focal mechanisms. The *P* axis and *T* axis using the *exact method* of FSMI software (Gephart, 1990) are indicated. Bathymetry map is derived from GEBCO2014 database.

Catalogue (Dziewonski et al., 1981; Ekström et al., 2012). This is consistent with the sinistral strike-slip between the Scotia and the South American plates (Galindo-Zaldívar et al., 1996; Giner-Robles et al., 2003; Pelayo & Wiens, 1989).

In order to identify the present-day stress, we analyzed earthquake focal mechanism data from Pelayo and Wiens (1989), the U.S. Geological Survey National Earthquake Information Centre (USGS, 2013), the Harvard Seismology Centroid Moment Tensor Catalogue (Dziewonski et al., 1981; Ekström et al., 2012), and Bollini and Sabbione (2014). The data include 56 events with magnitudes between 4.2 and 7 (Figure 10). The analysis of the earthquake focal mechanisms using the *exact method* of FSMI software (Gephart, 1990) gives for Tierra del Fuego and the northern Scotia Arc (inset in Figure 9a) a NE-SW subhorizontal *P* axis (trend/plunge: 056/10) and orthogonal *T* axis (trend/plunge: 325/05). The axial ratio (*R*) is about 0.35 (Rb = 0.35), supporting a triaxial stress compatible with the strike-slip and reverse-oblique fault types associated, in turn, with the individual focal mechanism and with the transpressional left-lateral regime that occurs along the North Scotia Ridge.

Geodetic studies determining recent displacement rates on Tierra del Fuego show an NE-SW direction, congruent with the compressional direction established from the earthquake focal mechanisms. The displacement direction is N036E south of the Fagnano Lake and N011E in the north (Mendoza et al., 2011, 2015). The horizontal velocities average 1.3 cm/a (Mendoza et al., 2011, 2015). The strongest deformation is concentrated along the Magallanes-Fagnano Fault System, approximately 30-km wide (Mendoza et al., 2011). The shortening orientation is NNE-SSW to NE-SW, and the extensional orientation is NW-SE (Mendoza et al., 2011), compatible with the left lateral movement of the Magallanes-Fagnano Fault System and the earthquake focal mechanisms obtained. Finally, the slip-rate reported from GPS data along the Fault System varies closely between 6.6 ± 1.3 (Smalley et al., 2003) and 4.4 ± 0.6 mm/a.

6. Conclusions

From the analysis of fracture data measured at 22 sites in Tierra del Fuego a total of 28 paleostress tensors have been obtained. In addition, 56 earthquake focal mechanisms were analyzed to determine the present-day orientations. The direction of σ_1 displays E-W to ESE-WNW and NE-SW main modes with most of the stress tensors having Rb relationships within a wrench regime close to an axial compressional regime. The orientation of σ_3 shows four modes oriented N-S, NE-SW, ESE-WNW, and NW-SE, whose Rb relationships indicate a tendency to radial tensional regime. Present-day stress orientation in the study zone shows NE-SW P axis and orthogonal NW-SE T axis with triaxial ellipsoids.

The stress orientations determined were interpreted in the tectonic context of Tierra del Fuego:

1. The closure of the Rocas Verdes basin during the Late Cretaceous involved first-order thrusting and folding of the continental margin under a contractional stress regime with NE-SW direction. Local deviations of the stress tensors were related to the orogenic curve of the backstop of the Andean chain that rotated

the initially formed fractures, and caused a change in the direction of the local stresses at the orogenic front, from NE-SW to almost NNW-SSE to NNE-SSW.

2. From the latest Cretaceous to the early Neogene, the effect of the interaction between the Río Chico Arch and the advance of the Fuegian fold-and-thrust belt is registered by the different stress orientations. The western area of the study zone shows a predominantly NE-SW orientation of σ_1, while in the eastern sector of the Mitre Peninsula recess the stress shows a main NW-SE average direction of compressive stress. That is, the stress trajectories converge toward the Río Chico Arch basement promontory.
3. After the late Miocene, the left-lateral movement of the Magallanes-Fagnano Fault System is congruent with a regional NE-SW compressive stress field. This stress field shows some deviations of its trajectory along the Magallanes-Fagnano Fault System, as seen in some sites near the fault zone in the northern and southern blocks, where the stress trajectories deviate from a NE-SW direction to E-W.
4. Many tensional tensors appear to postdate the contractional structures of the Fuegian Andes. In these cases they could be related with an episode of late Cenozoic regional uplift in Tierra del Fuego and southern Patagonia suggested by previous research. The late Cenozoic uplift could have caused some extent of collapse of the mountain belt through extensional deformation, explaining the tensional and radial tensional regimes determined in some sites. In other cases, the tensional tensors show subparallelism between superposed σ_1 and σ_3 trajectories, which in turn are parallel to folds and perpendicular to thrusts. We explain the tensional stresses in this context as the effect of local extension due to the mechanics of thrusts and associated folds formed by bending.
5. Finally, the present-day stress field in the Tierra del Fuego and the northern Scotia Arc is characterized by a NE-SW subhorizontal P axis.

Acknowledgments

The data supporting Figures 3–7 and 9 are available in supporting information Figure S1 and Tables S1–S3 (Bollini & Sabbione, 2014; Bott, 1959; Dziewonski et al., 1981; Ekström et al., 2012; Gephart & Forsyth, 1984; Orife & Lisle, 2006; Pelayo & Wiens, 1989; USGS, 2013). This study is dedicated to the memory of Pedro Ibarra, who sadly passed away on 8 August 2018. He will be in our hearts forever. Rest in peace. The authors acknowledge the collaboration of E. Olivero, D. Martinioni, M. Barbagallo and M. Pérez (CADIC-CONICET), and A. Imbert during the field work. Permission to work in Parque Nacional Tierra del Fuego was granted by APN project 049-DRPA. We also thank Ian W. D. Dalziel, Mauricio Calderón, José Luis Simón, three anonymous reviewers, and the Editors Claudio Faccenna and Laurent Jolivet for their constructive feedback. This work has been funded by projects CTM2011-30241-C02-02, CTM2014-60451-C2-2-P and CTM2017-89711-C2-2-P of the Spanish R&D National Plan and by PICT funding from ANPCyT-FONCyT (Argentina). Jean Sanders is thanked for reviewing the English text.

References

Aleksandroski, P., Inderhaug, O. H., & Knapstad, B. (1992). Tectonic structures and wellbore breakout orientation, in 33rd US Symposium on Rock Mechanics, edited by J.R. Tillerson and W. Wawersik, Santa Fe, A.A. Balkema Publishers, Rotterdam, the Netherlands, 29-37.

Angelier, J. (1979). Determination of the mean principal directions of stresses for a given fault population. *Tectonophysics*, *56*, T17–T26.

Angelier, J., & Mechler, P. (1977). Sur Une méthode graphique de recherche des contraintres principales également utilisable en tectonique et en séismologie: la méthode des diédres droits. *Bulletin de la Société Géologique de France*, *7*(19), 1309–1318.

Arlegui, L. E., & Simón, J. L. (1998). Reliability of palaeostress analysis from fault striations in near multidirectional extension stress fields. Example from the Ebro Basin, Spain. *Journal of Structural Geology*, *20*, 827–840.

Armijo, R., Tapponier, P., & Mercier, J. L. (1986). Quaternary extension in southern Tibet: Field observations and tectonic implications. *Journal of Geophysical Research*, *91*, 13,803–13,872. https://doi.org/10.1029/JB091iB14p13803

Barker, P. F. (2001). Scotia Sea tectonic evolution: Implications for mantle flow and palaeocirculation. *Earth Science Reviews*, *55*, 1–39. https://doi.org/10.1016/S0012-8252(01)00055-1

Bergerat, F., & Vandycke, S. (1994). Palaeostress analysis and geodynamical implications of Cretaceous-Tertiary faulting in Kent and the Boulonnais. *Journal of the Geological Society of London*, *151*, 439–448. https://doi.org/10.1144/gsjgs.151.3.0439

Biddle, K. T., Uliana, M. A., Mitchum, R. M., Fitzgerald, M. G., & Wright, R. C. (1986). The stratigraphic and structural evolution of the central and eastern Magallanes Basin, southern South America. In P. A. Allen & P. Homewood (Eds.), *Foreland basins* (Vol. 8, pp. 41–61). Oxford, UK: Blackwell Ltd.

Bohoyo, F., Galindo-Zaldívar, J., Jabaloy, A., Maldonado, A., Rodríguez-Fernández, J., Schreider, A., & Suriñach, E. (2007). Extensional deformation and development of deep basins associated with the sinistral transcurrent fault zone of the Scotia-Antarctic plate boundary. *Geological Society, London, Special Publications*, *290*, 203–217. https://doi.org/10.1144/SP290.6

Bollini, C., & Sabbione, N. (2014). Moment tensor solution for a M 4.2 event in Tierra del Fuego. *Earth Sciences Research Journal*, *18*, 170–171.

Bott, M. H. P. (1959). The mechanics of oblique slip faulting. *Geological Magazine*, *96*, 109–117. https://doi.org/10.1017/S0016756800059987

Calderón, M., Fosdick, J. C., Warren, C., Massonne, H.-J., Fanning, C. M., Fadel Cury, L., et al. (2012). The lowgrade Canal de las Montañas shear zone and its role on the tectonic emplacement of the Sarmiento ophiolitic complex and Late Cretaceous Patagonian Andes orogeny, Chile. *Tectonophysics*, *524-525*, 165–185.

Calderón, M., Hervé, F., Fuentes, F., Fosdick, J. C., Sepúlveda, F., & Galaz, G. (2016). Tectonic evolution of Paleozoic and Mesozoic Andean metamorphic complexes and the Rocas Verdes ophiolites in southern Patagonia. In M. C. Ghiglione (Ed.), *Geodynamic evolution of the southernmost Andes. Connections with the Scotia Arc* (pp. 7–36). Switzerland: Springer Earth System Sciences. https://doi.org/10.1007/978-3-319-39727-6

Calderón, M., Prades, C. F., Hervé, F., Avendaño, V., Fanning, C. M., Massone, H.-J., et al. (2013). Petrological vestiges of the Late Jurassic–Early Cretaceous transition from rift to back-arc basin in southernmost Chile: New age and geochemical data from the Capitán Aracena, Carlos III, and Tortuga ophiolitic complexes. *Geochemical Journal*, *47*, 201–217.

Casas, A. M., Gil, M. A., & Simón, J. L. (1990). Los métodos de análisis de paleoesfuerzos a partir de poblaciones de fallas: Sistemática y técnicas de aplicación. *Estudios Geológicos*, *46*, 385–398.

Casas, A. M., & Maestro, A. (1996). Deflection of a compressional stress field by large-scale basement faults. A case study from the Tertiary Almazán basin Spain. *Tectonophysics*, *255*, 135–156. https://doi.org/10.1016/0040-1951(95)00111-5.

Casas, A. M., Serón, F. J., & Simón, J. L. (1992). Stress deflection in a tectonic compressional field: A model for the Northwestern Iberian Chain, Spain. *Journal of Geophysical Research*, *97*, 7183–7192. https://doi.org/10.1029/91JB02292

Cooper, M. (1992). The analysis of fracture systems in subsurface thrust structures from the Foothills of the Canadian Rockies. In K. R. McClay (Ed.), *Thrust tectonics* (pp. 391–406). Chapman & Hall.

Cosgrove, J., & Ameen, M. (2000). A comparison of geometry spatial organization and fracture patterns associated with forced folds and buckle folds. In J. W. Cosgrove & M. S. Ameen (Eds.), *Forced Folds and Fractures, Sp. Pub*, (Vol. 169 pp. 7–21). London: Geological Society.
Cunningham, W. D. (1995). Orogenesis at the southern tip of the Americas: The structural evolution of the Cordillera Darwin metamorphic complex, southernmost Chile. *Tectonophysics*, *244*, 197–229. https://doi.org/10.1016/0040-1951(94)00248-8
Dalziel, I. W. D. (1986). Collision and Cordilleran orogenesis: An Andean perspective. *Geological Society London Special Publications*, *19*, 389–404. https://doi.org/10.1144/GSL.SP.1986.019.01.22
Dalziel, I. W. D., De Wit, M. F., & Palmer, K. F. (1974). Fossil marginal basin in the southern Andes. *Nature*, *250*, 291–294. https://doi.org/10.1038/250291a0
Dalziel, I. W. D., Dott, R. H., Winn, R. D. Jr., & Bruhn, R. L. (1975). Tectonic relations of South Georgia Island to the southernmost Andes. *Geological Society of America Bulletin*, *86*, 1034–1040. https://doi.org/10.1130/0016-7606(1975)86.
Dávila, F. M., Lithgow-Bertelloni, C., Martina, F., Ávila, P., Nóbile, J., Collo, G., et al. (2018). Mantle influence on Andean and pre-Andean topography. In A. Folguera, et al. (Eds.), *The evolution of the Chilean-Argentinean Andes* (pp. 363–385). Cham: Springer International Publishing. https://doi.org/10.1007/978-3-319-67774-3_15
Delvaux, D., Moeys, R., Stapel, G., Petit, C., Levi, K., Miroshnichenko, A., et al. (1997). Paleostress reconstructions and geodynamics of the Baikal region, Central Asia, Part 2. Cenozoic rifting. *Tectonophysics*, *282*, 1–38.
Diraison, M., Cobbold, P., Gapais, D., Rossello, E., & Le Corre, C. (2000). Cenozoic crustal thickening, wrenching and rifting in the foothills of the southernmost Andes. *Tectonophysics*, *316*, 91–119. https://doi.org/10.1016/S0040-1951(99)00255-3
Dziewonski, A. M., Chou, T.-A., & Woodhouse, J. H. (1981). Determination of earthquake source parameters from waveform data for studies of global and regional seismicity. *Journal of Geophysical Research*, *86*, 2825–2852. https://doi.org/10.1029/JB086iB04p02825
Ekström, G., Nettles, M., & Dziewonski, A. M. (2012). The global CMT project 2004–2010: Centroid-moment tensors for 13,017 earthquakes. *Physics of the Earth and Planetary Interiors*, *200-201*, 1–9. https://doi.org/10.1016/j.pepi.2012.04.002
Engelder, T., & Geiser, P. (1980). On the use of regional joint sets as trajectories of paleostress fields during the development of the Appalachian Plateau, New York. *Journal of Geophysical Research*, *85*(B11), 6319–6341. https://doi.org/10.1029/JB085iB11p06319
Etchecopar, A. (1984). Etude des états de contrainte en tectonique cassante et simulations de déformations plastiques (approchc mathématique). M.S. thesis, U.S.T.L. Montpellier, Montpellier, France.
Etchecopar, A., Vasseur, G., & Daignieres, M. (1981). An inverse problem in microtectonics for the determination of stress tensors from fault population analysis. *Journal of Structural Geology*, *3*, 51–65. https://doi.org/10.1016/0191-8141(81)90056-0
Eyal, Y., & Reches, Z. (1983). Tectonic analysis of the Dead Sea Rift regions since the Late Cretaceous based on mesostructures. *Tectonics*, *2*, 167–185. https://doi.org/10.1029/TC002i002p00167
Galeazzi, J. S. (1998). Structural and stratigraphic evolution of the western Malvinas Basin, Argentina. *AAPG Bulletin*, *82*, 596–636.
Galindo-Zaldívar, J., Bohoyo, F., Maldonado, A., Schreider, A., Suriñach, E., & Vázquez, J. T. (2006). Propagating rift during the opening of a small oceanic basin: The Protector Basin (Scotia Arc, Antarctica). *Earth and Planetary Science Letters*, *241*, 398–412. https://doi.org/10.1016/j.epsl.2005.11.056
Galindo-Zaldívar, J., & González-Lodeiro, F. (1988). Faulting phase differentiation by means of computer search on a grid pattern. *An-Tec*, *2*, 90–97.
Galindo-Zaldívar, J., Jabaloy, A., Maldonado, A., & Sanz de Galdeano, C. (1996). Continental fragmentation along the South Scotia Ridge transcurrent plate boundary (Antarctic Peninsula). *Tectonophysics*, *259*, 275–301. https://doi.org/10.1016/0040-1951(95)00211-1
Geiser, P. A. (1988). The role of kinematics in the construction and analysis of geological cross-sections in deformed terrains. *Geological Society of America*, *222*, 47–76. https://doi.org/10.1130/SPE222-p47
Gephart, J. W. (1990). FMSI: A Fortran program for inverting fault/slickenside and earthquake focal mechanism data to obtain the regional stress tensor. *Computational Geosciences*, *16*, 953–989. https://doi.org/10.1016/0098-3004(90)90105-3
Gephart, J. W., & Forsyth, D. W. (1984). An improved method for determining the regional stress tensor using earthquake focal mechanism data: Application to the San Fernando earthquake sequence. *Journal of Geophysical Research*, *89*, 9305–9320. https://doi.org/10.1029/JB089iB11p09305
Ghiglione, M. C., Quinteros, J., Yagupsky, D., Bonillo-Martínez, P., Hlebszevtich, J., Ramos, V. A., et al. (2010). Structure and tectonic history of the foreland basins of southernmost South America. *Journal of South American Earth Sciences*, *29*, 262–277. https://doi.org/10.1016/j.jsames.2009.07.006
Ghiglione, M. C., Ramos, V., Cuitiño, J., & Barberón, V. (2016). Growth of the southern Patagonian Andes (46–53°S) and its relation with subduction processes. In A. Folguera, M. Naipauer, L. Sagripanty, M. C. Ghiglione, D. Orts, & L. B. Giambiagi (Eds.), *Growth of the Southern Andes* (pp. 201–240). Switzerland: Springer Earth System Sciences. https://doi.org/10.1007/978-3-319-23060-3_10
Giner-Robles, J. L., González-Casado, J. M., Gumiel, P., Martín-Velázquez, S., & García-Cuevas, C. (2003). A kinematic model of the Scotia plate (SW Atlantic Ocean). *Journal of South American Earth Sciences*, *16*, 179–191. https://doi.org/10.1016/S0895-9811(03)00064-6
Gordillo, S., Bujalesky, G. G., Pirazzoli, P. A., Rabassa, J. O., & Saliège, J.-F. (1992). Holocene raised beaches along the northern coast of the Beagle Channel, Tierra del Fuego, Argentina. *Palaeogeography, Palaeoclimatology, Palaeoecology*, *99*, 41–54. https://doi.org/10.1016/0031-0182(92)90006-Q
Hancock, P. L. (1985). Brittle microtectonics: Principles and practice. *Journal of Structural Geology*, *7*, 437–457. https://doi.org/10.1016/0191-8141(85)90048-3
Hancock, P. L., & Engelder, T. (1989). Neotectonic joints. *Bulletin Geological Society of America*, *101*, 1197–1208. https://doi.org/10.1130/0016-7606(1989)101.
Heidbach, O., Reinecker, J., Tingay, M., Müller, B., Sperner, B., Fuchs, K., & Wenzel, F. (2007). Plate boundary forces are not enough: Second- and third-order stress patterns highlighted in the World Stress Map database. *Tectonics*, *26*, TC6014. https://doi.org/10.1029/2007TC0022133
Heidbach, O., Tingay, M., Barth, A., Reinecker, J., Kurfess, D., & Müller, B. (2010). Global crustal stress pattern based on the world stress map database release 2008. *Tectonophysics*, *482*, 3–15.
Homberg, C., Angelier, J., Bergerat, F., & Lacombe, O. (2004). Using stress deflections to identify past ruptures in fault systems. *Earth and Planetary Science Letters*, *217*, 409–424. https://doi.org/10.1016/S0012-821X(03)00586-7.
Homberg, C., Hu, J. C., Angelier, J., Bergerat, F., & Lacombe, O. (1997). Characterization of stress perturbations near major fault zones: Insights from 2-D distinct-element numerical modelling and field studies (Jura mountains). *Journal of Structural Geology*, *19*(5), 703–718.
Ivins, E. R., & James, T. S. (2004). Bedrock response to Llanquihue Holocene and present-day glaciation in southernmost South America. *Geophysical Research Letters*, *31*, L24613. https://doi.org/10.1029/2004GL021500
Klepeis, K. A. (1994). The Magallanes and Deseado fault zones; major segments of South American-Scotia transform plate boundary in southernmost South America, Tierra del Fuego. *Journal of Geophysical Research*, *99*, 22. https://doi.org/10.1029/94JB01749

Klepeis, K. A., Betka, P., Clarke, G., Fanning, M., Hervé, F., Rojas, L., et al. (2010). Continental underthrusting and obduction during the Cretaceous closure of the Rocas Verdes rift basin, Cordillera Darwin, Patagonian Andes. *Tectonics*, *29*, TC3014. https://doi.org/10.1029/2009TC002610

Lacombe, O. (2012). Do fault slip data inversions actually yield "paleostresses" that can be compared with contemporary stresses? A critical discussion. C. R. *Geoscience*, *344*, 159–173.

Larter, R. D., Vanneste, L. E., Morris, P., & Smythe, D. K. (2003). Structure and tectonic evolution of the South Sandwich arc. In R. D. Larter & P. T. Leat (Eds.), *Intra-oceanic subduction systems: tectonic and magmatic processes* (Vol. 219 pp. 255–284). London: Geological Society, London, Special Publications.

Lemiszki, P. J., Landes, J. D., & Hatcher, R. D. (1994). Controls on hinge-parallel extension fracturing in single-layer tangential-longitudinal strain folds. *Journal of Geophysical Research*, *99*(B11), 22,027–22,041. https://doi.org/10.1029/94JB01853

Lisle, R. J., Orife, T., & Arlegui, L. (2001). A stress inversion method requiring only faults slip sense. *Journal of Geophysical Research*, *106*(B2), 2281–2289. https://doi.org/10.1029/2000JB900353

Lodolo, E., Menichetti, M., Bartole, R., Ben-Avraham, Z., Tassone, A., & Lippai, H. (2003). Magallanes-Fagnano continental transform fault (Tierra del Fuego, southernmost South America). *Tectonics*, *22*(6), 1076. https://doi.org/10.1029/2003TC001500

Lund Snee, J.-E., & Zoback, M. D. (2016). State of stress in Texas: Implications for induced seismicity. *Geophysical Research Letters*, *43*, 10,208–10,214. https://doi.org/10.1002/2016GL070974

Maestro, A., & López-Martínez, J. (2011). Cenozoic stress field in the southern Wright Peninsula (Adelaide Island) from brittle mesostructures population analysis. *Polish Polar Research*, *32*(1), 39–58. https://doi.org/10.2478/v10183-011-0006-8.

Maestro, A., López-Martínez, J., Galindo-Zaldívar, J., Bohoyo, F., & Mink, S. (2014). Evolution of the stress field in the southern Scotia Arc from the late Mesozoic to the present-day. *Global and Planetary Change*, *123*, 269–297. https://doi.org/10.1016/j.gloplacha.2014.07.023

Maffione, M., Speranza, F., Faccenna, C., & Rossello, E. (2010). Paleomagnetic evidence for a pre-early Eocene (~50 Ma) bending of the Patagonian orocline (Tierra del Fuego, Argentina): Paleogeographic and tectonic implications. *Earth and Planetary Science Letters*, *289*, 273–286. https://doi.org/10.1016/j.epsl.2009.11.015

Maldonado, A., Balanyá, J. C., Barnolas, A., Galindo-Zaldívar, J., Hernández-Molina, F. J., Jabaloy, A., et al. (2000). Tectonics of an extinct ridge-transform intersection, Drake Passage (Antarctica). *Marine Geophysical Researches*, *21*, 43–68.

Maloney, K. T., Clarke, G. L., Klepeis, K. A., Fanning, C. M., & Wang, W. (2011). Crustal growth during back-arc closure: Cretaceous exhumation history of Cordillera Darwin, southern Patagonia. *Journal of Metamorphic Geology*, *29*, 649–672. https://doi.org/10.1111/j.1525-1314.2011.00934.x

Marshak, S., Wilkerson, M., & Hsui, T. (1992). Generation of curved fold-thrust belts: Insight from simple physical and analytical models. In K. R. McClay (Ed.), *Thrust Tectonics* (pp. 83–93). London: Chapman & Hall.

Martínez-Peña, M. B., Casas-Sainz, A. M., & Millán-Garrido, H. (1995). Palaeostress associated with thrust sheet emplacement and related folding in southern central Pyrenees, Huesca, Spain. *Journal of the Geological Society of London*, *152*, 353–364. https://doi.org/10.1144/gsjgs.152.2.0353

Mendoza, L., Perdomo, R., Hormaechea, J. L., Del Cogliano, D., Fritsche, M., Richter, A., & Dietrich, R. (2011). Present-day crustal deformation along the Magallanes-Fagnano Fault System in Tierra del Fuego from repeated GPS observations. *Geophysical Journal International*, *184*, 1009–1022. https://doi.org/10.1111/j.1365-246X.2010.04912.x

Mendoza, L., Richter, A., Fritsche, M., Hormaechea, J. L., Perdomo, R., & Dietrich, R. (2015). Block modeling of crustal deformation in Tierra del Fuego from GNSS velocities. *Tectonophysics*, *651-652*, 58–65. https://doi.org/10.1016/j.tecto.2015.03.013

Mooney, W. D. (1989). Seismic methods for determining earthquake source parameters and lithospheric structure. In L. C. Pakiser & W. D. Mooney (Eds.), *Geophysical framework of the continental United States* (Vol. 172, pp. 71–110). Boulder, CO: Geological Society of America Memoir.

Müller, B., Zoback, M. L., Fuchs, K., Mastin, L., Gregersen, S., Pavoni, N., et al. (1992). Regional patterns of tectonic stress in Europe. *Journal of Geophysical Research*, *97*, 11,783–11,803. https://doi.org/10.1029/91JB01096

Mukasa, S. B., & Dalziel, I. W. D. (1996). Southernmost Andes and South Georgia Island, North Scotia Ridge: Zircon U-Pb and muscovite 40Ar39Ar age constraints on tectonic evolution of Southwestern Gondwanaland. *Journal of South American Earth Sciences*, *9*(5–6), 349–365. https://doi.org/10.1016/S0895-9811(96)00019-3

Nelson, E. P. (1982). Post-tectonic uplift of the cordillera Darwin orogenic core complex: Evidence from fission track geochronology and closing temperature-time relationships. *Journal of the Geological Society*, *139*, 755–761. https://doi.org/10.1144/gsjgs.139.6.0755

Nelson, E. P., Dalziel, I. W. D., & Milnes, A. G. (1980). Structural geology of the Cordillera Darwin-Collisional-style orogenesis in the southernmost Chilean Andes. *Eclogae Geologicae Helvetiae*, *73*, 727–751. https://doi.org/10.5169/seals-164987.

Olaiz, A. J., Muñoz-Martín, A., De Vicente, G., Vegas, R., & Cloetingh, S. (2009). European continuous active tectonic strain-stress map. *Tectonophysics*, *474*, 33–40.

Olivero, E. B., & Malumián, N. (2008). Mesozoic-Cenozoic stratigraphy of the Fuegian Andes, Argentina. *Geologica Acta*, *6*(1), 5–18.

Olivero, E. B., & Martinioni, D. R. (2001). A review of the geology of the Argentinian Fuegian Andes. *Journal of South American Earth Sciences*, *14*, 175–188. https://doi.org/10.1016/S0895-9811(01)00016-5

Orife, T., & Lisle, R. J. (2006). Assessing the statistical significance of palaeostress estimates: Simulations using random fault-slips. *Journal of Structural Geology*, *28*, 952–956.

Pedrera, A., Galindo-Zaldívar, J., Ruiz-Constán, A., Bohoyo, F., Torres-Carbonell, P., Ruano, P., et al. (2014). The last major earthquakes along the Magallanes-Fagnano fault system recorded by disturbed trees (Tierra del Fuego, South America). *Terra Nova*, *26*(6), 448–453. https://doi.org/10.1111/ter.12119

Pelayo, A., & Wiens, D. A. (1989). Seismotectonics and relative plate motions in the Scotia Sea region. *Journal of Geophysical Research*, *94*, 7293–7320. https://doi.org/10.1029/JB094iB06p07293

Pérez, L. F., Bohoyo, F., Hernández-Molina, F. J., Casas, D., Galindo-Zaldívar, J., Ruano, P., & Maldonado, A. (2016). Tectonic activity evolution of the Scotia-Antarctic Plate boundary from mass transport deposit analysis. *Journal of Geophysical Research: Solid Earth*, *121*, 2216–2234. https://doi.org/10.1002/2015JB012622

Poblete, F., Roperch, P., Arriagada, C., Ruffet, G., de Arellano, C. R., Hervé, F., & Poujol, M. (2016). Late cretaceous-early Eocene counter-clockwise rotation of the Fueguian Andes and evolution of the Patagonia-Antarctic Peninsula system. *Tectonophysics*, *668-669*, 15–34. https://doi.org/10.1016/j.tecto.2015.11.025

Poblete, F., Roperch, P., Hervé, F., Diraison, M., Espinoza, M., & Arriagada, C. (2014). The curved Magallanes fold and thrust belt: Tectonic insights from a paleomagnetic and anisotropy of magnetic susceptibility study. *Tectonics*, *33*, 2526–2551. https://doi.org/10.1002/2014TC003555

Ponce, J. J., Olivero, E. B., & Martinioni, D. R. (2008). Upper Oligocene-Miocene clinoforms of the foreland Austral Basin of Tierra del Fuego, Argentina: Stratigraphy, depositional sequences and architecture of the foredeep deposits. *Journal of South American Earth Sciences*, *26*, 36–54. https://doi.org/10.1016/j.jsames.2007.12.001

Ramsay, J. G., & Huber, M. I. (1983). *The techniques of modern structural geology, Volume 2: Folds and fractures*. London: Academic Press.

Rapalini, A. E., Peroni, J., Luppo, T., Tassone, A., Cerredo, M. E., Esteban, F., et al. (2015). Palaeomagnetism of Mesozoic magmatic bodies of the Fuegian Cordillera: Implications for the formation of the Patagonian Orocline. *Geological Society - Special Publications*, *425*. https://doi.org/10.1144/sp425.3

Reches, Z. (1978). Analysis of faulting in three-dimensional strain fields: II. *Theoritical analysis. Tectonophysics*, *95*(1–2), 133–156. https://doi.org/10.1016/0040-1951(83)90264-0.

Reynolds, S. D., Mildren, S. D., Hillis, R. R., Meyer, J. J., & Flottmann, T. (2005). Maximum horizontal stress orientations in the Cooper Basin, Australia: Implications for plate-scale tectonics and local stress sources. *Geophysical Journal International*, *160*, 331–343.

Robbiano, J. A., Arbe, H. A., & Gangui, A. (1996). Cuenca Austral Marina. In V. A. Ramos, & M. A. Turic (Eds.), *Geología y recursos naturales de la Plataforma Continental Argentina, Geología y recursos naturales de la Plataforma Continental Argentina, Relatorio del XIII Congreso Geológico Argentino y III Congreso de Exploración de Hidrocarburos* (pp. 323–341). Buenos Aires.: Asociación Geológica Argentina, Instituto Argentino del Petróleo.

Simón, J. L. (1984). Compresión y distensión alpinas en la Cadena Ibérica Oriental. M.S. thesis, Univ. Zaragoza, Zaragoza, Spain.

Simón, J. L. (1986). Analysis of gradual change in stress regime (example from the eastern Iberian Chain, Spain). *Tectonophysics*, *124*(1-2), 37–53. https://doi.org/10.1016/0040-1951(86)90136-8

Simón, J. L. (2018). Forty years of paleostress analysis: Has it attained maturity? *Journal of Structural Geology*. https://doi.org/10.1016/j.jsg.2018.02.011

Simón, J. L., Arlegui, L. E., Cortés, A. L., Liesa, C. L., & Maestro, A. (2000). Evaluación de la calidad de los tensores de esfuerzos: el índice IQ. *Geotemas*, *1*(1), 83–86.

Smalley, R., Kendrick, E., Bevis, M. G., Dalziel, I. W. D., Taylor, F., Lauría, E., et al. (2003). Geodetic determination of relative plate motion and crustal deformation across the Scotia-South America plate boundary in eastern Tierra del Fuego. *Geochemistry, Geophysics, Geosystems*, *4*(9), 1070. https://doi.org/10.1029/2002GC000446

Smith, W. H. F., & Sandwell, D. Y. (1997). Global seafloor topography from satellite altimetry and ship depth sounding. *Science*, *277*, 1957–1962. https://doi.org/10.1126/science.277.5334.1956

Sperner, B., & Zweigel, P. (2010). A plea for more caution in fault–slip analysis. *Tectonophysics*, *482*, 29–41.

Srivastava, D. C., & Engelder, T. (1990). Crack-propagation sequence and the pore-fluid conditions during thefault-bend folding in the Appalachian Valley and Ridge, Pennsylvania. *Geological Society of America Bulletin*, *102*, 116–128.

Sue, C., & Ghiglione, M. C. (2016). Wrenching tectonism in the southernmost Andes and the Scotia Sea constrained from fault kinematic and seismotectonic overviews. In M. C. Ghihlione (Ed.), *Geodynamic evolution of the southernmost Andes. Connections with the Scotia Arc* (pp. 137–171). London: Springer Earth System Sciences. https://doi.org/10.1007/978-3-319-39727-6

Tapponier, P., & Molnar, P. (1976). Slip-line field theory and large-scale continental tectonics. *Nature*, *164*, 319–324. https://doi.org/10.1038/264319a0

Tassone, A., Lippai, H., Lodolo, E., Menichetti, M., Comba, A., Hormaechea, J. L., & Vilas, J. F. (2005). A geological and geophysical crustal section across the Magallanes-Fagnano fault in Tierra del Fuego. *Journal of South American Earth Sciences*, *19*, 99–109. https://doi.org/10.1016/j.jsames.2004.12.003

Tingay, M. R. P., Müller, B., Reinecker, J., & Heidbach, O. (2006). State and origin of the present-day stress field in sedimentary basins: New results from the World Stress Map Project. 41st U.S. Symposium on Rock Mechanics (USRMS): 50 Years of Rock Mechanics - Landmarks and Future Challenges, held in Golden, Colorado, June 17-21.

Torres Carbonell, P. J., Cao, S. J., & Dimieri, L. V. (2017). Spatial and temporal characterization of progressive deformation during orogenic growth: Example from the Fuegian Andes, southern Argentina. *Journal of Structural Geology*, *99*, 1–19. https://doi.org/10.1016/j.jsg.2017.04.003

Torres Carbonell, P. J., & Dimieri, L. V. (2013). Cenozoic contractional tectonics in the Fuegian Andes, southernmost South America: A model for the transference of orogenic shortening to the foreland. *Geologica Acta*, *11*, 359–370. https://doi.org/10.1344/105.000001874.

Torres Carbonell, P. J., Dimieri, L. V., & Martinioni, D. R. (2013). Early foreland deformation of the Fuegian Andes (Argentina): Constraints from the strain analysis of Upper Cretaceous-Danian sedimentary rocks. *Journal of Structural Geology*, *48*, 14–32. https://doi.org/10.1016/j.jsg.2012.12.010

Torres Carbonell, P. J., Dimieri, L. V., Olivero, E. B., Bohoyo, F., & Galindo-Zaldívar, J. (2014). Structure and tectonic evolution of the Fuegian Andes (southernmost South America) in the framework of the Scotia Arc development. *Global and Planetary Change*, *123*, 174–188. https://doi.org/10.1016/j.gloplacha.2014.07.019

Torres Carbonell, P. J., Guzmán, C., Yagupsky, D., & Dimieri, L. V. (2016). Tectonic models for the Patagonian orogenic curve (southernmost Andes): An appraisal based on analog experiments from the Fuegian thrust-fold belt. *Tectonophysics*, *671*, 76–94. https://doi.org/10.1016/j.tecto.2016.01.020

Torres Carbonell, P. J., Olivero, E. B., B, E., & Dimieri, L. V. (2008). Control en la magnitud de desplazamiento de rumbo del Sistema Transformante Fagnano, Tierra del Fuego, Argentina. *Revista Geologica de Chile*, *35*, 63–77. https://doi.org/10.4067/S0716-02082008000100003

Torres Carbonell, P. J., Rodríguez Arias, L., & Atencio, M. R. (2017). Geometry and kinematics of the Fuegian thrust-fold belt, southernmost Andes. *Tectonics*, *36*, 33–50. https://doi.org/10.1002/2016tc004349

Turner, J. P., & Hancock, P. L. (1989). Relationship between thrusting and joint systems in the Jaca thrust-top basin, Spanish Pyrenees. *Journal of Structural Geology*, *12*, 217–226. https://doi.org/10.1016/0191-8141(90)90006-K

United States Geological Survey (USGS) (2013). Database of National Earthquake Information Center. Retrieved from http://www.neic.cr.usgs.gov/[cited 1-11-2016

Wojtal, S., & Pershing, J. (1991). Paleostresses associated with faults of large offset. *Journal of Structural Geology*, *13*, 49–62. https://doi.org/10.1016/0191-8141(91)90100-W

Yale, D. P., Rodriguez, J. M., & Mercer, T. B. (1994). In-situ stress orientation and the effects of local structure-Scott Field, North Sea. In *Eurock'94* (pp. 945–952). Rotterdam, Netherlands: A.A. Balkema Publishers.

Yrigoyen, M. (1989). Cuenca de Malvinas. In G. A. Chebli & L. A. Spalletti (Eds.), *Cuencas Sedimentarias Argentinas, Serie Correlación Geológica*, edited by, (pp. 481–491). Tucumán: Universidad Nacional de Tucumán, Instituto Superior de Correlación Geológica.

Zoback, M. L. (1992). First- and second-order patterns of stress in the lithosphere: The world stress map project. *Journal of Geophysical Research*, *97*, 11,703–11,728. https://doi.org/10.1029/92JB00132